

Generalized Stability Analyses of Asymmetric Disturbances in One- and Two-Celled Vortices Maintained by Radial Inflow

DAVID S. NOLAN

Department of Mathematics, Lawrence Berkeley National Laboratory, Berkeley, California

BRIAN F. FARRELL

Department of Earth and Planetary Sciences, Harvard University, Cambridge, Massachusetts

(Manuscript received 11 July 1997, in final form 27 May 1998)

ABSTRACT

The dynamics of both transient and exponentially growing disturbances in two-dimensional vortices that are maintained by the radial inflow of a fixed cylindrical deformation field are investigated. Such deformation fields are chosen so that both one-celled and two-celled vortices may be studied. The linearized evolution of asymmetric perturbations is expressed in the form of a linear dynamical system $d\mathbf{x}/dt = \mathbf{A}\mathbf{x}$. The shear of the mean flow results in a nonnormal dynamical operator \mathbf{A} , allowing for the transient growth of perturbations even when all the modes of the operator are decaying. It is found that one-celled vortices are stable to asymmetric perturbations of all azimuthal wavenumbers, whereas two-celled vortices can have low-wavenumber instabilities. In all cases, generalized stability analysis of the dynamical operator identifies the perturbations that grow the fastest, both instantaneously and over a finite period of time. While the unstable modal perturbations necessarily convert mean-flow vorticity to perturbation vorticity, the perturbations with the fastest instantaneous growth rate use the deformation of the mean flow to rearrange their vorticity fields into configurations with higher kinetic energy. Also found are perturbations that use a hybrid of these two mechanisms to achieve substantial energy growth over finite time periods.

Inclusion of the dynamical effects of radial inflow—vorticity advection and vorticity stretching—is found to be extremely important in assessing the potential for transient growth and instability in these vortices. In the two-celled vortex, neglecting these terms destabilizes the vortex for azimuthal wavenumbers one and two. In the one-celled vortex, neglect of the radial inflow terms results in an overestimation of transient growth for all wavenumbers, and it is also found that for high wavenumbers the maximum transient growth decreases as the strength of the radial inflow increases.

The effects of these perturbations through eddy flux divergences on the mean flow are also examined. In the one-celled vortex it is found that for all wavenumbers greater than one the net effect of most perturbations, regardless of their initial configuration, is to increase the kinetic energy of the mean flow. As these perturbations are sheared over they cause upgradient eddy momentum fluxes, thereby transferring their kinetic energy to the mean flow and intensifying the vortex. However, for wavenumber one in the one-celled vortex, and all wavenumbers in the two-celled vortex, it was found that nearly all perturbations have the net effect of decreasing the kinetic energy of the mean flow. In these cases, the kinetic energy of the perturbations accumulates in nearly neutral or unstable modal structures, so that energy acquired from the mean flow is not returned to the mean flow but instead is lost through dissipation.

1. Introduction

In this report we introduce a new approach to the study of the dynamics of asymmetries in primarily axisymmetric intense atmospheric vortices—such as waterspouts, tornadoes, and hurricanes. For waterspouts and tornadoes, these asymmetries include low-level wind shear, the unsteady and asymmetric supply of their

angular momentum, and also the effects of turbulence. The success of recent three-dimensional numerical simulations in reproducing realistic maximum tornado wind speeds (Lewellen et al. 1997), compared with the much lower velocities predicted by theories and simulations based on axisymmetric models (Lilly 1969; Fiedler and Rotunno 1986; Fiedler 1994), indicates that asymmetries may play an important role in the maintenance of an intense and robust tornadic vortex. For hurricanes, asymmetric forcing includes the beta effect, potential vorticity anomalies in the mid- and upper levels of the atmosphere, and the shear of environmental winds; these asymmetries are believed to play a significant role in the track and intensity changes of these cyclones (Mol-

Corresponding author address: David S. Nolan, Department of Atmospheric Science, Colorado State University, Fort Collins, CO 80523.
E-mail: nolan@chandra.atmos.colostate.edu

inari 1992; Shapiro 1992; Montgomery and Farrell 1993; Smith and Weber 1993).

The traditional approach to understanding the behavior of nearly axisymmetric vortices has relied heavily on hydrodynamic stability analyses of their azimuthal velocity profiles, which in practice are approximated as a function of radius, either from measurements or from idealized functions (such as a Rankine vortex). A classical stability analysis is applied to small perturbations linearized about the mean azimuthal flow. Examples of this kind of analysis include those of Michaelke and Timme (1967), Rotunno (1978), Staley and Gall (1979), Gall (1983, 1985), and more recently Steffens (1988), Flierl (1988), and Peng and Williams (1991). In accordance with traditional notions of stability in shear flows originally derived by Rayleigh (1880), most of these reports found that a change in sign of the vorticity gradient of the azimuthal wind was necessary for the existence of instability. Some of the analyses cited above also included the effects of a radially varying vertical wind that can create additional instabilities.

In recent years a new approach has been taken to the study of asymmetric dynamics in tropical cyclones, which relies on the analysis of such perturbations as an initial-value problem rather than as an eigenvalue problem. Carr and Williams (1989) and Smith and Montgomery (1995) found linearized equations for the evolution of asymmetric disturbances in hurricane-like vortex flows, while Guinn and Schubert (1993) also included the results of numerical simulations of perturbed nondivergent barotropic flows in their analyses. The results of these studies show that asymmetric disturbances generally decay rapidly with time due to the strong shear of the vortex, and that these decay rates increase with both the azimuthal and radial wavenumbers of the disturbances. Kallenbach and Montgomery (1995) also demonstrated how such disturbances can undergo a period of transient growth before decaying. Asymmetric dynamics have also been investigated by Willoughby (1992, 1995) for their role in determining tropical cyclone tracks, in regard to both the northwest drift of barotropic vortices due to the poleward increase of the Coriolis parameter, and to how these asymmetries can be used to determine the initial motion of the vortex in forecast models. The growth of asymmetric disturbances near the cores of tropical cyclones has also been advocated as the cause of the polygonal eyewall phenomenon (Schubert et al. 1999).

A simplifying assumption of great potential importance to the dynamics that was made in these stability studies of intense atmospheric vortices was neglecting the convergent background flow—the radial inflow—which forms and maintains these vortices. While initially this was justified by the belief that the radial velocities in the core of these vortices was negligible, it is now well known due to laboratory experiments (Wan and Chang 1972), theoretical analyses (Burgraff et al. 1971), and axisymmetric numerical simulations (How-

ells, et al. 1988) that there is in fact a strong radial inflow near the surface in tornadic vortices, with radial velocities typically half as large as the azimuthal velocities. At some point as it approaches the central axis of the vortex, the radial inflow separates from the surface, turns upward, and flows up and out of the vortex core. (Note: by the “core” of the vortex we mean inside, and in the vicinity of, the radius of maximum winds.) Hurricanes are also known to have substantial radial inflow velocities in the surface boundary layer, from both observations (Franklin et al. 1993) and numerical simulations (Shapiro 1992; Liu et al. 1997). Using a very high-resolution simulation of Hurricane Andrew (1992), Liu et al. also found small (order $1\text{--}2\text{ m s}^{-1}$) radial inflow velocities outside the eyewall in the middle levels, as did Shapiro (1992) in his three-level model. While these velocities are very small compared to the maximum azimuthal wind speeds, our results will show that small radial inflow velocities can have a measurable impact on asymmetric dynamics.

It is easy to imagine that this radial inflow may have important effects on the stability of these vortices. For example, one possible effect of this radial inflow could be to advect growing perturbations out of the region of maximum shear and inside the vortex core before it can grow substantially. In this sense, the radial inflow may render all growing perturbations “transient” by suppressing modal instability.

In this report we introduce a general method for determining the stability of two-dimensional vortex flows that includes the radial inflow that maintains the vortex. Furthermore, we will use an extension of classical stability analysis, known as generalized stability analysis, to examine the growth of both transient and exponentially growing (if they exist) perturbations on the mean flow. Then we will examine specifically how these perturbations interact with the mean flow and the effects of radial inflow on the dynamics. In section 2 we will give an introduction to generalized stability analysis; in section 3 we will describe our models of the idealized vortices under consideration; in section 4 we derive equations for the evolution of linearized asymmetric perturbations to these flows; in section 5 we will evaluate and comment on the stability of these vortices; in section 6 we will find the transient perturbations that grow the most in finite times; in section 7 we will investigate how these perturbations interact with the mean flow and how the presence of the radial inflow affects the results; and in section 8 we will discuss our conclusions.

2. Generalized stability theory

While the traditional approach to assessing the stability of observed flows in fluid dynamics and meteorology has been restricted to determining whether the flow supports exponentially growing modes, in recent years an alternative approach has de-

veloped. Inspired by the observation of Thompson (1887) and Orr (1907) that properly configured disturbances in stable shear flows undergo a finite period of energy growth before decaying, Farrell (1982) demonstrated the growth of baroclinic disturbances of this type in the atmospheric midlatitude jet. The possibility of transient growth in the absence of exponentially growing modes is expressed mathematically by the non-normality of the linearized dynamical operator, that is, the fact that the dynamical operator does not commute with its transpose. Such transient growth may not be trivial: in Poiseuille flow at Reynolds number 5000, Butler and Farrell (1992) found disturbances that could grow in energy by a factor of 4897, despite the fact that Poiseuille flow is exponentially stable at this Reynolds number. This understanding has led to a general analysis of nonnormal systems that has since been used extensively to understand transient growth in deformation and shear flows (Farrell 1988, 1989; Butler and Farrell 1992; Farrell and Ioannou 1993a, 1993b, 1996). Consideration of both transient and exponential growth processes has come to be called *generalized stability analysis*.

Let us describe in some detail how the nonnormality of a system can lead to transient growth. First we write down the evolution of disturbances as a linear dynamical system:

$$\frac{d\mathbf{y}}{dt} = \mathbf{T}\mathbf{y}, \tag{2.1}$$

where \mathbf{y} is a function or vector that describes the state of the perturbation(s), and \mathbf{T} is the time evolution operator. We also define a positive-definite Hermitian operator \mathbf{M} such that the energy of the system can be written

$$E = \mathbf{y}^*\mathbf{M}\mathbf{y}. \tag{2.2}$$

We now perform the following useful change into generalized velocity coordinates \mathbf{x} :

$$\mathbf{x} = \mathbf{M}^{1/2}\mathbf{y}, \tag{2.3}$$

$$\mathbf{A} = \mathbf{M}^{1/2}\mathbf{T}\mathbf{M}^{-1/2}, \tag{2.4}$$

so that in generalized velocity coordinates,

$$\frac{d\mathbf{x}}{dt} = \mathbf{A}\mathbf{x}, \tag{2.5}$$

$$E = \mathbf{x}^*\mathbf{x}. \tag{2.6}$$

Equation (2.4) is a similarity transformation, so the eigenvalues of \mathbf{A} are the same as the eigenvalues of \mathbf{T} . If all the eigenvalues of \mathbf{T} have a negative real part, then all the modes of \mathbf{T} are decaying. So then are all the modes of \mathbf{A} , and we can conclude that the energy of the system goes to zero as $t \rightarrow \infty$. The structure in these generalized velocity coordinates that dominates energetically for large times will be the eigenvector of \mathbf{A} associated with the eigenvalue with the largest real part, which we will call the *least damped mode* (LDM).

The structure of the LDM in the original coordinate system \mathbf{y} can be found by transforming back into the original coordinates, that is, inverting (2.3).

This does not address the issue of the energetics of the system when $0 \leq t < \infty$. We can easily solve for the instantaneous rate of change in energy:

$$\begin{aligned} \frac{\partial E}{\partial t} &= \frac{\partial}{\partial t}(\mathbf{x}^*\mathbf{x}) = \left(\frac{\partial}{\partial t}\mathbf{x}^*\right)\mathbf{x} + \mathbf{x}^*\left(\frac{\partial \mathbf{x}}{\partial t}\right) \\ &= \mathbf{x}^*\mathbf{A}^\dagger\mathbf{x} + \mathbf{x}^*\mathbf{A}\mathbf{x} = \mathbf{x}^*(\mathbf{A}^\dagger + \mathbf{A})\mathbf{x}, \end{aligned} \tag{2.7}$$

where the \dagger refers to the Hermitian matrix transpose. Because the energy operator $(\mathbf{A}^\dagger + \mathbf{A})$ is normal and Hermitian, the eigenvector of $(\mathbf{A}^\dagger + \mathbf{A})$ with the largest eigenvalue will be at any instant the fastest growing (or least decaying) perturbation. This is certain because the eigenvectors of a normal matrix are complete and orthogonal—any other perturbation that does not project onto the dominant eigenvector could be constructed entirely from the other eigenvectors, all of which grow more slowly than the first. Such fastest growing perturbations are usually called the *instantaneous optimals* (IOs) of the system. By setting $\mathbf{x} = \mathbf{e}_{\max}$ (the eigenvector with maximum eigenvalue) in Eq. (2.7), one can see that this upper bound on the normalized energy growth rate is

$$\left(\frac{1}{E} \frac{\partial E}{\partial t}\right)_{\max} = \lambda_{\max}, \tag{2.8}$$

where λ_{\max} is the largest eigenvalue of $(\mathbf{A}^\dagger + \mathbf{A})$.

In regards to the issue of transient growth and non-normality, consider that when \mathbf{A} is normal, \mathbf{A} and \mathbf{A}^\dagger have the same eigenvectors. Therefore the IO will be the same as the LDM, and its rate of change of energy will be twice the real part of the eigenvalue of the LDM. When \mathbf{A} is nonnormal, the eigenvalues and eigenvectors of \mathbf{A} and the energy operator will be different, and any positive eigenvalues of the energy operator will correspond to transient growth as indicated by (2.8).

One can also find the perturbations of maximum growth over finite time, which we call *finite time optimals* (FTOs). The energy as a function of time is

$$E(t') = \mathbf{x}^*(t')\mathbf{x}(t') = \mathbf{x}^*(0)e^{\mathbf{A}^\dagger t'}e^{\mathbf{A}t'}\mathbf{x}(0). \tag{2.9}$$

Because the matrix product in (2.9) is normal and Hermitian, we see again that the eigenvector corresponding to the largest eigenvalue of $e^{\mathbf{A}^\dagger t'}e^{\mathbf{A}t'}$ will have the largest growth (or smallest decay) in energy between $t = 0$ and $t = t'$. We have that

$$\left(\frac{E(t')}{E(0)}\right)_{\max} = \lambda_{\max}, \tag{2.10}$$

where here λ_{\max} is the maximum eigenvalue of the matrix product $e^{\mathbf{A}^\dagger t'}e^{\mathbf{A}t'}$. Another approach to finding FTOs uses the singular value decomposition (SVD) of the propagator matrix $e^{\mathbf{A}t'}$. The propagator matrix can be decomposed as

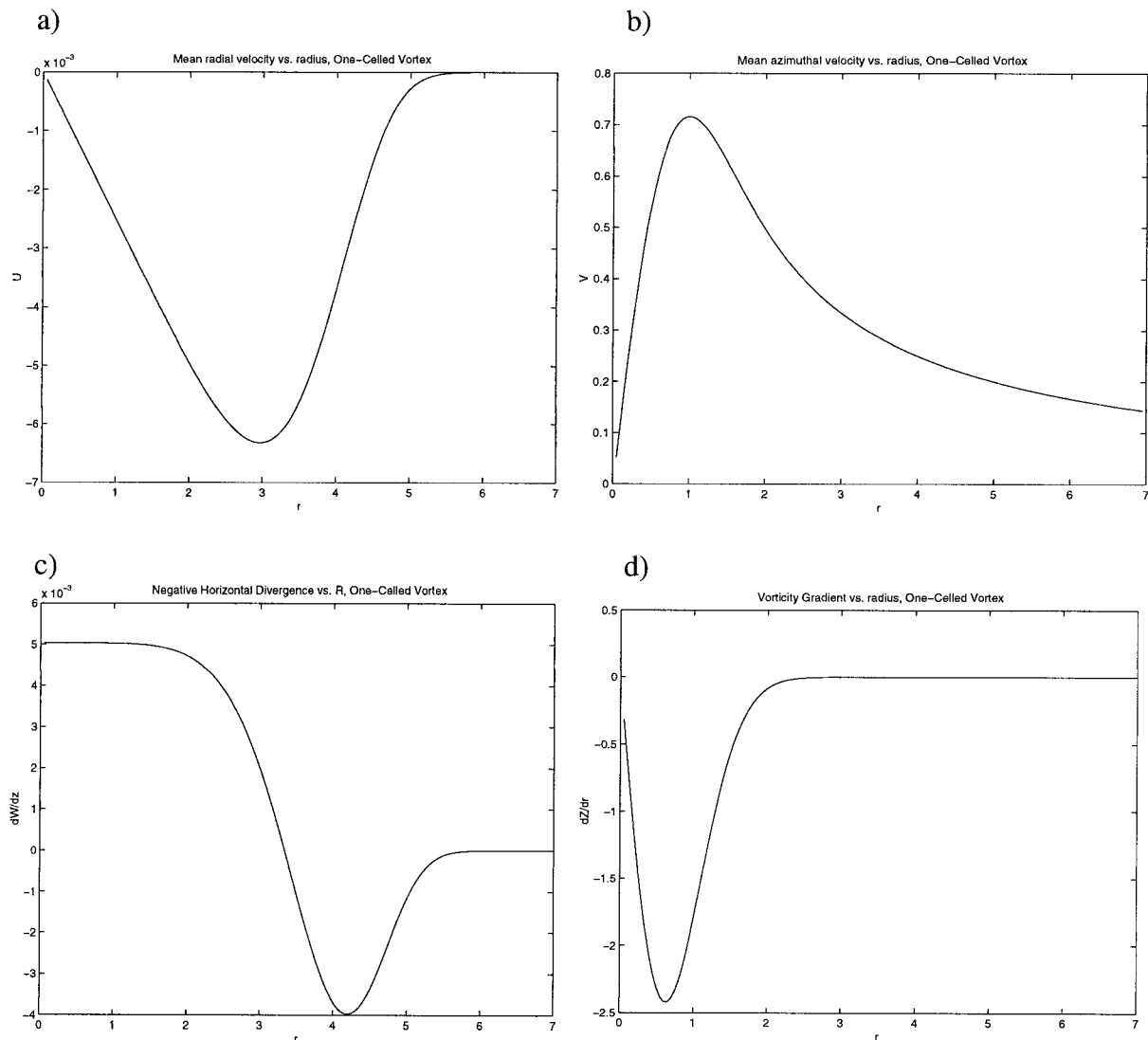


FIG. 1. Profiles of radial and azimuthal velocity for the idealized one-celled vortex: (a) radial velocity, (b) azimuthal velocity, (c) negative horizontal divergence (stretching), (d) vorticity gradient.

$$e^{At} = \mathbf{U}\mathbf{D}\mathbf{V}^\dagger, \quad (2.11)$$

where \mathbf{U} and \mathbf{V} are unitary matrices that can be interpreted to represent orthogonal decompositions of the domain and the range of the propagator, and \mathbf{D} is a positive-definite diagonal matrix, the values of which represent the relative excitation of the system by their corresponding basis vectors. We can then write

$$e^{A^\dagger t} e^{At} = \mathbf{V}\mathbf{D}\mathbf{U}^\dagger \mathbf{U}\mathbf{D}\mathbf{V}^\dagger = \mathbf{V}\mathbf{D}^2 \mathbf{V}^\dagger. \quad (2.12)$$

Clearly by previous argument the basis vector associated with the largest value of \mathbf{D} will result in the most energy growth at time t , and the magnitude of the excitation will be the square of the largest element of \mathbf{D} . The SVD method is also useful in that the maximal state of the

FTO is produced in \mathbf{U} simultaneously with its initial condition in \mathbf{V} .

3. One-celled and two-celled vortices maintained by radial inflow in a closed domain

As stated in the introduction we will investigate the dynamics of steady two-dimensional vortex flows that are generated when a cylindrical deformation field acts on a rotating fluid. In the following sections we will outline a method for finding such steady-state solutions given an arbitrary deformation field, and show how to choose such fields so as to produce either one-celled or two-celled vortices.

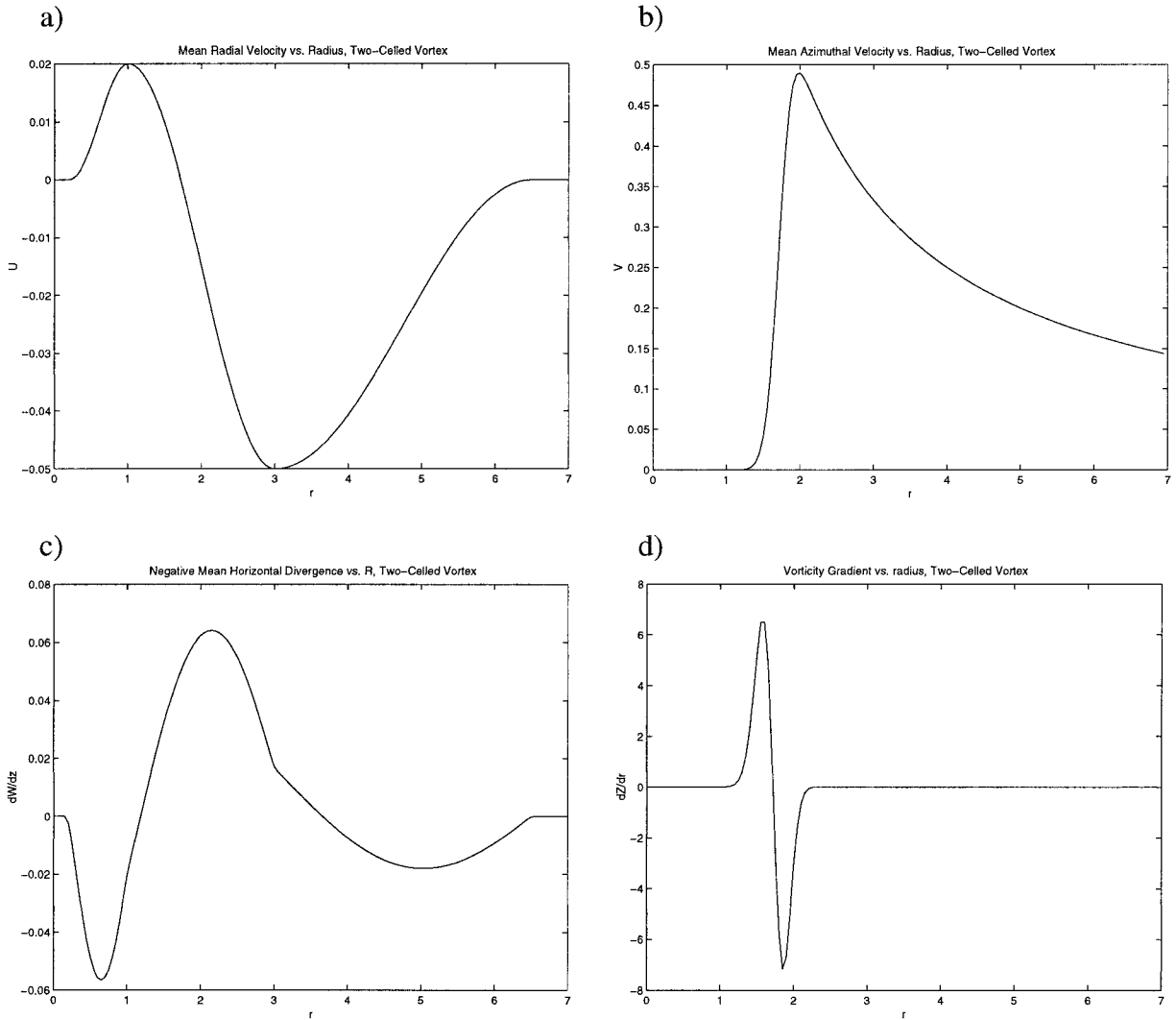


FIG. 2. Profiles of radial and azimuthal velocity for the idealized two-celled vortex: (a) radial velocity, (b) azimuthal velocity, (c) negative horizontal divergence (stretching), (d) vorticity gradient.

a. Formulation of the steady-state solution in arbitrary deformation fields

The classic example of one such cylindrically symmetric flow is the well-known Burgers' vortex solution [Burgers (1948), also known as the Burgers–Rott solution, see Rott (1958)]. If there exists in an unbounded domain a cylindrical deformation field of the form

$$U = -\frac{1}{2}\alpha r, \tag{3.1}$$

$$W = \alpha z, \tag{3.2}$$

where U and W refer to the radial and vertical velocities in cylindrical coordinates, then a steady-state solution of the Navier–Stokes equations is obtained when the azimuthal velocity is

$$V(r) = \frac{\Gamma_\infty}{2\pi r} \left[1 - \exp\left(-\frac{\alpha r^2}{4\nu}\right) \right], \tag{3.3}$$

where Γ_∞ is the circulation at infinity and ν is the kinematic viscosity. Note that this azimuthal velocity profile for small r approaches solid-body rotation, and for large r asymptotes to a potential vortex ($V = \Gamma_\infty/2\pi r$).

Suppose instead we assume an arbitrary cylindrical deformation field based on a radial inflow velocity field that is a function of r only:

$$U = U(r). \tag{3.4}$$

By continuity, we have

$$\frac{\partial W}{\partial z} = -\frac{1}{r} \frac{\partial}{\partial r}(rU), \tag{3.5}$$

so that the vertical velocity field $W(r, z)$ may be deter-

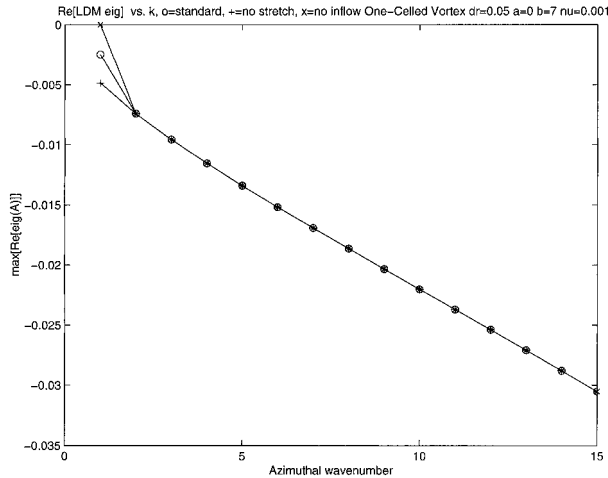


FIG. 3. Real parts of the eigenvalues of the LDM for azimuthal wavenumbers 1–15 in the one-celled vortex: ○—standard case with inflow; +—with stretching term removed; ×—with stretching and advection removed.

mined up to constant. Holding the U and W velocities fixed, we can write down a single advection–diffusion equation for the evolution of the axisymmetric azimuthal velocity V

$$\begin{aligned} \frac{\partial V}{\partial t} + U \frac{\partial V}{\partial r} + W \frac{\partial V}{\partial z} + \frac{UV}{r} \\ = \nu \left(\frac{\partial^2 V}{\partial r^2} + \frac{1}{r} \frac{\partial V}{\partial r} - \frac{V}{r^2} \right). \end{aligned} \quad (3.6)$$

If the azimuthal velocity field is a function of r only, the vertical advection term may be neglected.

Now let us turn our attention to the solution of (3.6) in the finite domain $0 \leq r \leq b$, with boundary conditions $V(0) = 0$ and $V(b) = V_b$. We discretize V onto equally spaced grid points between $r = 0$ and $r = b$, and write these values as the column vector \mathbf{V} . Using matrix representations of standard finite-difference operators, (3.6) may be represented as the inhomogeneous linear system

$$\frac{\partial \mathbf{V}}{\partial t} = \mathbf{A} \mathbf{V} + \mathbf{B}, \quad (3.7)$$

where \mathbf{B} is a column vector that allows us to incorporate the boundary conditions. Our steady-state solution is found by solving for \mathbf{V} such that its time derivative is zero:

$$\mathbf{V} = -\mathbf{A}^{-1} \mathbf{B}. \quad (3.8)$$

Examples of some solutions of (3.8) are shown in the following sections.

b. One-celled vortices

While the Burgers' vortex solution is a useful point of reference, the fact that it resides in an unbounded domain creates serious difficulties for the analysis of

asymmetric perturbations in this flow. The greatest difficulties are those associated with the inflow of fluid through the edge of the domain at $r = b$. Let us instead create a deformation field similar to the Burgers' vortex deformation field, except that its support lies entirely within a cylinder of radius $r = b$; we will use $b = 7$ for the rest of this work. Furthermore, we require that the radial inflow velocity transitions very smoothly to zero as we approach the outer boundary, and is nearly zero for a substantial region near the outer boundary. An example of such a radial inflow function is given by

$$U(r) = -\alpha r e^{-\mu r^6}. \quad (3.9)$$

This function with $\alpha = 5.0 \times 10^{-3}$ and $\mu = 2.44 \times 10^{-4}$ is shown in Fig. 1a. This particular choice for α , in conjunction with a choice of $\nu = 0.001$ for the viscosity, sets the radius of maximum winds $r_{\max} = 1$ for Burgers' vortex solution (3.3). Using this radial velocity field and an outer boundary condition on V such that the circulation at the outer boundary $\Gamma_b = 2\pi r_b V_b = 2\pi$ (i.e., the circulation of the fluid at the edge of the domain is equal to 2π everywhere), (3.6) results in the solution shown in Fig. 1b. The vortex Reynolds number, as it is usually defined, is $\text{Re}_\nu = r_b V_b / \nu = 1000$. This solution, which has $r_{\max} = 1.0$ and maximum azimuthal velocity $v_{\max} = 0.71$, is virtually identical to the Burgers' solution with the same parameters despite the fact that the radial inflow velocity transitions to zero near the outer edge of the domain. The stretching (or negative horizontal divergence) of the vertical velocity function is shown in Fig. 1c, and the radial gradient of the vertical vorticity is shown in Fig. 1d.

c. Two-celled vortices

In light of observations, laboratory experiments, and both axisymmetric and three-dimensional numerical simulations, it is generally believed that many tornadoes (and other atmospheric vortices) have a stagnant core, in which air flows down from above along the center axis, diverges horizontally at the surface, and then recirculates upward along the annulus defined by the radius of maximum winds. Such a flow has come to be called a "two-celled" vortex. Perhaps the most obvious example of a two-celled vortex in nature is the hurricane, which has a calm eye and generally descending motion inside the eyewall. Much like the Burgers' vortex for one-celled vortices, an analytic model for two-celled vortices was found by Sullivan (1959); unfortunately, it too only exists in an unbounded domain, and has the further disadvantage that due to diffusion the azimuthal velocity in the core is substantial. We instead present a simple model that produces a stagnant-core vortex in a finite domain. We define the radial velocity $U(r)$ to have inflow outside some radius, and outflow away from the $r = 0$ axis, with a stagnation point in between:

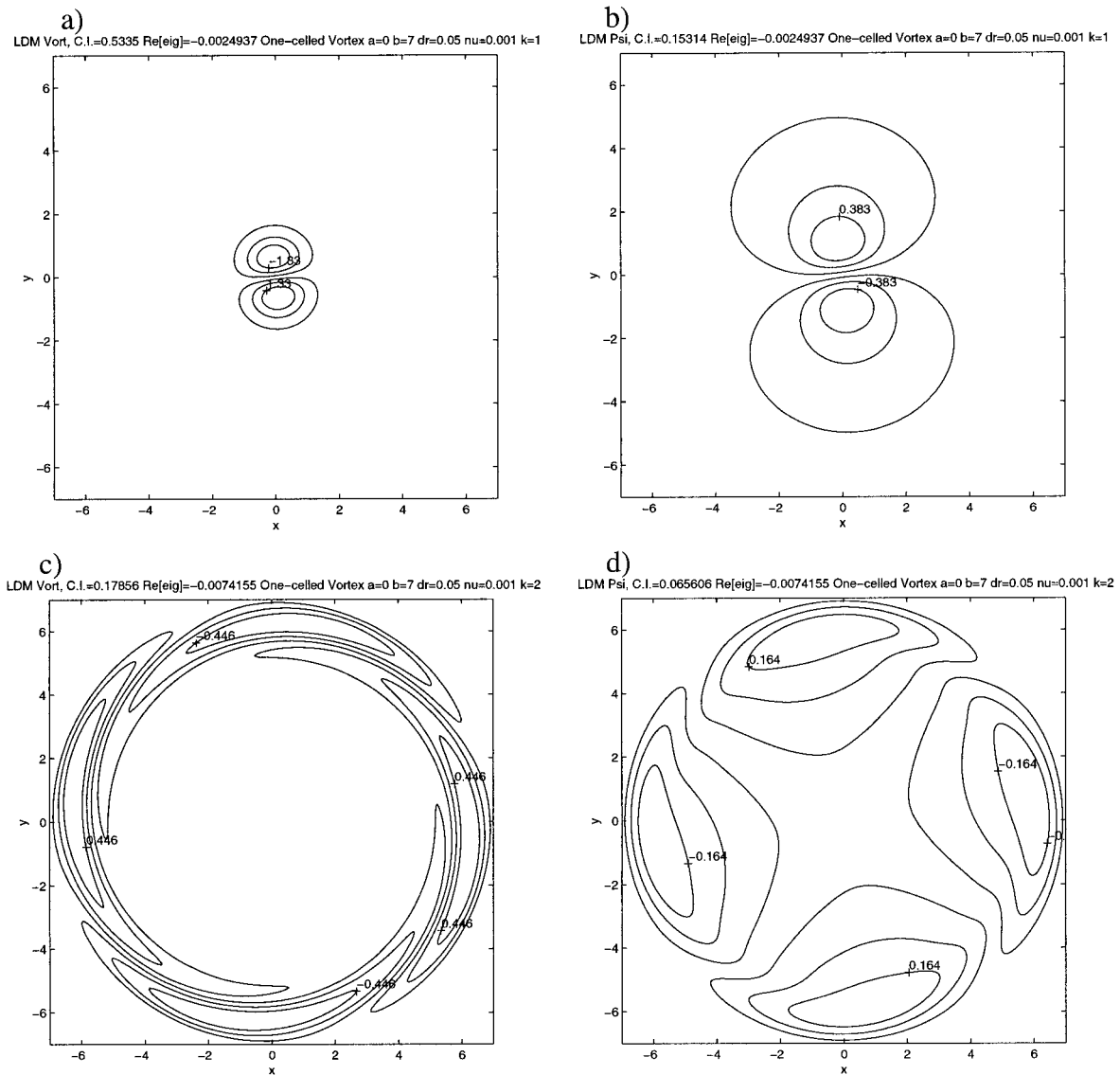


FIG. 4. The LDMs for the first two azimuthal wavenumbers in the one-celled vortex: (a) contours of vorticity for $k = 1$, (b) contours of streamfunction for $k = 1$, (c) contours of vorticity for $k = 2$, (d) contours of streamfunction for $k = 2$. The contour intervals and decay rates (the real part of the eigenvalue) are indicated at the top of each plot.

$$U(r) = \begin{cases} 0 & r < 0.2 \\ 0.02 \sin^2\left(\pi \frac{r - 0.2}{1.6}\right) & 0.2 < r < 1 \\ 0.035 \cos\left(\pi \frac{r - 1}{2.0}\right) - 0.15 & 1 < r < 3 \\ -0.05 \cos^2\left(\pi \frac{r - 3}{7.0}\right) & 3 < r < 6.5 \\ 0 & r > 6.5. \end{cases} \tag{3.10}$$

This radial velocity function is shown in Fig. 2a. Applying our method, where again we have defined the

circulation at the outer boundary $\Gamma_b = 2\pi$, and the viscosity $\nu = 0.001$ so that $Re_\nu = 1000$, we find the azimuthal velocity profile shown in Fig. 2b. The associated deformation function is shown in Fig. 2c, while the resulting vertical vorticity gradient is shown in Fig. 2d. We can see that outside the radius of maximum winds at $r = 2$, the velocity profile is nearly exactly that of a potential flow, while inside the radius of maximum winds the velocity quickly drops to zero and the inner core is stagnant. The vorticity gradient changes sign in the transition region $1 < r < 2$, where the flow transitions from the potential flow to the stagnant inner core, indicating the possibility for instability as predicted by Rayleigh's (1880) theorem for growing disturbances in inviscid rotating flows.

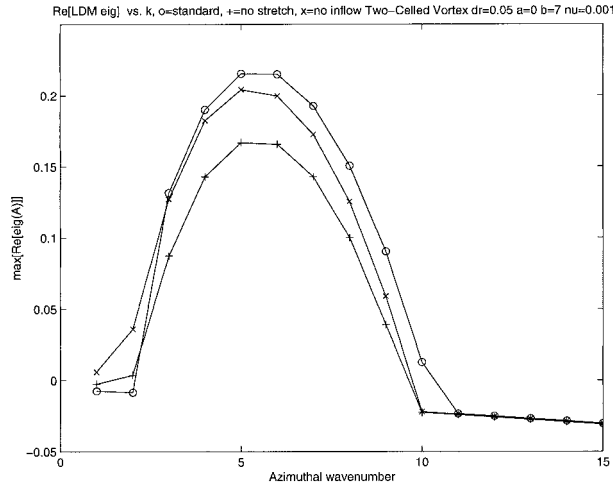


FIG. 5. Stability diagram for asymmetric perturbations on the two-celled vortex, showing the real parts of the LDMs for each azimuthal wavenumber from $k = 1$ to $k = 15$: \circ —standard case with inflow, $+$ —with stretching term removed, \times —with stretching and advection removed.

4. The evolution of vertical vorticity perturbations in idealized vortices with radial inflow

a. Mathematical models of wave-mean flow interactions near and inside the vortex core

Investigations of atmospheric vortex dynamics face the problem of using finite resources to investigate dynamics in an unbounded domain. Most work on vortex dynamics has used “solid wall” boundary conditions at some distance outside the vortex core to close the system (Howard and Gupta 1962; Staley and Gall 1979; Gall 1983; Staley and Gall 1984; Gall 1985; Steffens 1988; Peng and Williams 1991). This practice is analogous to the approximation of the midlatitude jet by bounded channel flows, and it is based on the reasonable assumption that disturbances to the mean flow that might lie outside of the “outer wall” will not unduly influence the results near or inside the vortex core. The results of such analyses have generally been consistent with results derived from unbounded solutions based on semi-analytic methods such as contour dynamics (Rotunno 1978; Flierl 1988), although Steffens (1988) did identify some significant changes in growth rates of a particular class of instabilities when the outer wall was moved farther away from the vortex core. We used this technique to limit the domain, and found through numerical experimentation that the location of the outer wall did not affect the important results (the kind of results that are affected by the location of the outer boundary are discussed below in section 5b).

b. The linearized evolution of vertical vorticity perturbations

The specific vortex flows we will study have been outlined in section 3, but generally speaking we wish

to describe the evolution of vertical vorticity perturbations in a swirling flow that has deformation and radial inflow that are functions of radius only. We restrict our attention to the dynamics of the vertical vorticity component ζ , in cylindrical coordinates, where it is assumed to have no variation in the vertical direction:

$$\frac{\partial \zeta}{\partial t} + u \frac{\partial \zeta}{\partial r} + \frac{v}{r} \frac{\partial \zeta}{\partial \theta} = \zeta \frac{\partial w}{\partial z} + \nu \left[\frac{\partial^2 \zeta}{\partial r^2} + \frac{1}{r} \frac{\partial \zeta}{\partial r} + \frac{1}{r^2} \frac{\partial^2 \zeta}{\partial \theta^2} \right]. \quad (4.1)$$

Now, we write each term in (4.1) as the sum of a radially varying mean and azimuthally, radially, and temporally varying perturbations: $u = U(r) + u'(r, \theta, t)$, $\zeta = Z(r) + \zeta'(r, \theta, t)$, and so on for v and w . Substituting these expressions into (4.1), we find the first-order equation for the perturbations:

$$\begin{aligned} \frac{\partial}{\partial t} \zeta' + U \frac{\partial}{\partial r} \zeta' + \Omega \frac{\partial}{\partial \theta} \zeta' + u' \frac{\partial Z}{\partial r} \\ = \zeta' \frac{\partial W}{\partial z} + \nu \left[\frac{\partial^2}{\partial r^2} + \frac{1}{r} \frac{\partial}{\partial r} + \frac{1}{r^2} \frac{\partial^2}{\partial \theta^2} \right] \zeta', \end{aligned} \quad (4.2)$$

where we have written Ω for the mean angular velocity V/r . The last term on the left-hand side represents the conversion of mean-flow vorticity to perturbation vorticity, which can result in instability.

Due to the azimuthal homogeneity of the background vortex, we can separate the solutions of (4.2) by writing them as a sum of harmonically varying azimuthal waves, that is, $\zeta'(r, \theta, t) = \sum_k \zeta_k(r, t) e^{ik\theta}$, and so on for the perturbations of u and v also. Substituting these forms into (4.2), we create for each wavenumber k a linear equation for the evolution of the radially and temporally varying vorticity function $\zeta_k(r, t)$:

$$\begin{aligned} \left(\frac{\partial}{\partial t} + U(r) \frac{\partial}{\partial r} + ik\Omega(r) \right) \zeta_k + u_k \frac{\partial Z}{\partial r} \\ = \zeta_k \frac{\partial W}{\partial z} + \nu \left[\frac{\partial^2 \zeta_k}{\partial r^2} + \frac{1}{r} \frac{\partial \zeta_k}{\partial r} - \frac{k^2}{r^2} \zeta_k \right]. \end{aligned} \quad (4.3)$$

From here on we will use the convention that the terms u_k , v_k , ζ_k refer to complex amplitude functions of r and t only.

c. The evaluation of velocities from the vorticity

As we can see from (4.3), when there is a nonzero background vorticity gradient, obtaining the evolution of the perturbation vorticity requires knowledge of the radial velocity perturbations. Furthermore, we anticipate the need to evaluate both u_k and v_k in the calculation of the perturbation kinetic energy and the eddy momentum fluxes. Following Carr and Williams (1989) and Smith and Montgomery (1995), we find the velocities by solving for the streamfunction:

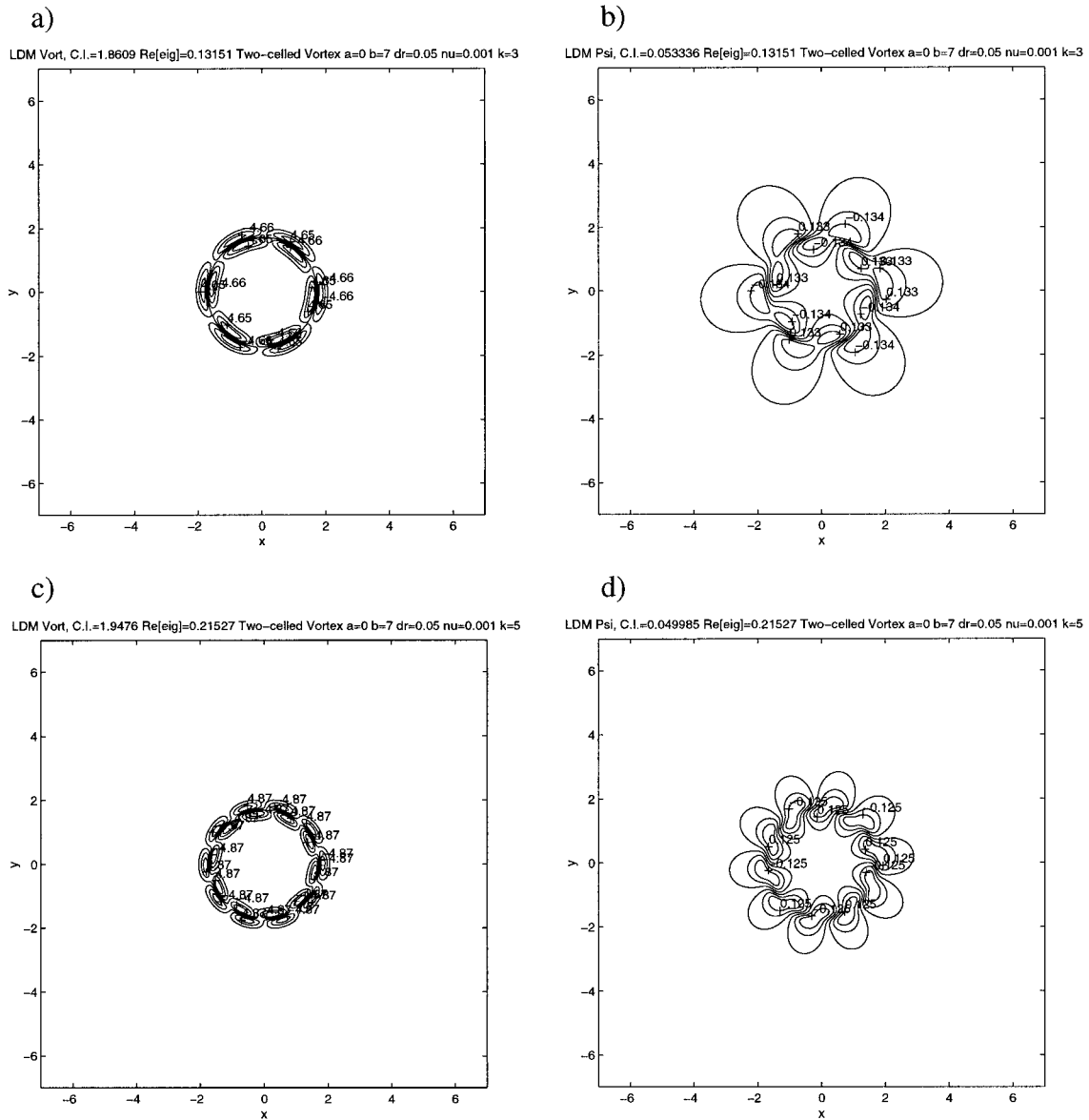


FIG. 6. Streamfunction and vorticity fields for the most unstable (least damped) perturbations at the first wavenumber with instability, $k = 3$, and the wavenumber with highest instability, $k = 5$: (a) $k = 3$ vorticity; (b) $k = 3$ streamfunction; (c) $k = 5$ vorticity; (d) $k = 5$ streamfunction.

$$\psi(r, \theta, t) = \sum_k \psi_k(r, t)e^{ik\theta} \tag{4.4}$$

$$u_k = \frac{-1}{r} \frac{\partial \psi_k}{\partial \theta} = \frac{-ik}{r} \psi_k \tag{4.5}$$

$$v_k = \frac{\partial \psi_k}{\partial r} \tag{4.6}$$

$$\begin{aligned} \zeta_k &= \frac{1}{r} \left[\frac{\partial}{\partial r} (rv_k) - \frac{\partial u_k}{\partial \theta} \right] \\ &= \left[\frac{\partial^2}{\partial r^2} + \frac{1}{r} \frac{\partial}{\partial r} - \frac{k^2}{r^2} \right] \psi_k. \end{aligned} \tag{4.7}$$

As previously discussed, we choose the boundary conditions of no normal flow at the outer boundary $r = b$; that is,

$$\psi_k(0, t) = \psi_k(b, t) = 0. \tag{4.8}$$

Given the vorticity, in the case of continuous functions Eq. (4.7) may be inverted with a Green's function:

$$\psi_k(r, t) = \int_a^b G_k(r, \rho) \zeta_k(\rho, t) d\rho. \tag{4.9}$$

The Green's function appropriate for this problem is [from Carr and Williams (1989), with the inner boundary a set to zero]

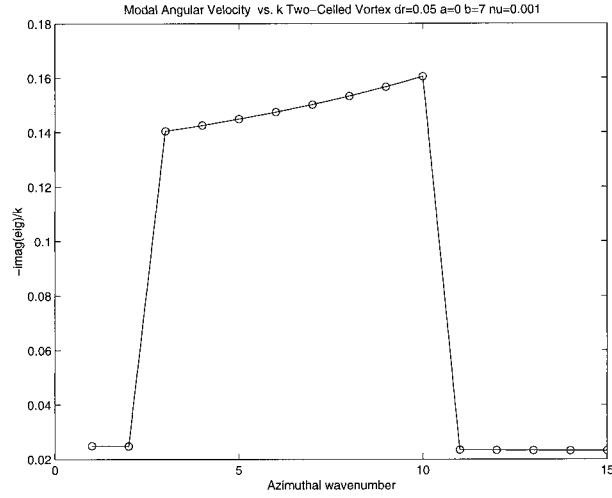


FIG. 7. Angular velocity, or phase speed, of the LDMs in the two-celled vortex for each azimuthal wavenumber from $k = 1$ to $k = 15$.

$$G_k(r, \rho) = \begin{cases} \frac{r^{2k}}{2kr^k b^{2k}} (\rho^{k+1} - b^{2k} \rho^{-k+1}) & 0 \leq r \leq \rho \\ \frac{r^{2k} - b^{2k}}{2kr^k b^{2k}} \rho^{k+1} & \rho \leq r \leq b. \end{cases} \quad (4.10)$$

d. The solution and analysis of the system

We would like to express the evolution of the perturbations as a linear dynamical system. We discretize the domain by assigning the values of the radial functions to evenly spaced points from $r = 0 + \Delta r$ to $r = b - \Delta r$, each point separated by a distance Δr . This converts the continuous radial functions into vectors of length $N = (b/\Delta r) - 1$. For all calculations we use $\Delta r = 0.05$ so that there are 139 grid points between the axis and the outer boundary. We express all derivatives as matrix operators corresponding to the usual centered-difference approximations, with the exception that the finite-difference operator used for the advection term is one-sided so that it represents a second-order upwinding advection scheme. We must also express the Green's function operation (4.9) as a matrix operation; that is,

$$\psi_k = \mathbf{G}_k \zeta_k, \quad (4.11)$$

where k refers to the wavenumber, and the operator \mathbf{G}_k is defined as above according to (4.9).

Finally, we take vorticity evolution equation (4.3) and manipulate it into a form with only the time derivative on the lhs, and install the matrix operators accordingly. The result is

$$\frac{d\zeta_k}{dt} = \mathbf{T}_k \zeta_k, \quad (4.12)$$

with

$$\mathbf{T}_k = -\mathbf{U}\mathbf{D}_{\text{up}} - ik\Omega + (\mathbf{DZ})ik\mathbf{R}^{-1}\mathbf{G}_k + \mathbf{S} + \nu(\mathbf{D}^2 + \mathbf{R}^{-1}\mathbf{D} - k^2\mathbf{R}^{-2}), \quad (4.13)$$

where we have written \mathbf{D} for the matrix representing the finite-difference calculation for the derivative with respect to r , \mathbf{D}_{up} for a similar but upwinded derivative operator, \mathbf{S} for the “stretching” term $\partial W/\partial z$, and (4.5) was used for the third term on the rhs. Operators that refer to functions of r only, such as the \mathbf{R}^{-1} operator, are simply diagonal matrices with the function values on the diagonal. We must also incorporate into the difference operators additional boundary conditions on the vorticity, which we choose to be

$$\zeta_k(0) = \zeta_k(b) = 0. \quad (4.14)$$

This condition prevents the advection and diffusion of perturbation vorticity into the domain from the boundaries. The solution of (4.12) in time is

$$\zeta_k(t) = e^{\mathbf{T}_k t} \zeta_k(0). \quad (4.15)$$

e. The kinetic energy of the perturbations

The kinetic energy for each perturbation in continuous space is

$$E = \int_0^b \left(\frac{\overline{u_k^2}}{2} + \frac{\overline{v_k^2}}{2} \right) 2\pi r dr, \quad (4.16)$$

where the overbars refer to averages around the azimuth of the real parts of the complex velocity functions. A streamfunction–vorticity formulation for the energy can be found by using (4.5)–(4.9) and integrating by parts to find

$$E = -\frac{1}{2} \int_0^b \overline{\psi_k \zeta_k} 2\pi r dr. \quad (4.17)$$

Using the fact that $\overline{pq} = \frac{1}{4}(p^*q + q^*p)$, we can rewrite (4.17) as

$$E = -\frac{\pi}{4} \int_0^b (\psi_k^* \zeta_k + \zeta_k^* \psi_k) r dr. \quad (4.18)$$

As discussed in section 2 it is useful to find an energy metric operator \mathbf{M} such that the energy of the discretized linear dynamical system may be written $E = \zeta^* \mathbf{M} \zeta$. For each azimuthal wavenumber k , the energy metric can be formulated from (4.18):

$$\mathbf{M}_k = \frac{-\pi\Delta r}{4} [\mathbf{G}_k^* \mathbf{R} + \mathbf{R} \mathbf{G}_k]. \quad (4.19)$$

5. Stability

a. The stability of the one-celled vortex

We first consider the one-celled vortex as described in section 3b. The nearly identical Burgers' vortex solution has been previously found to be stable to all two-dimensional disturbances by Robinson and Saffman

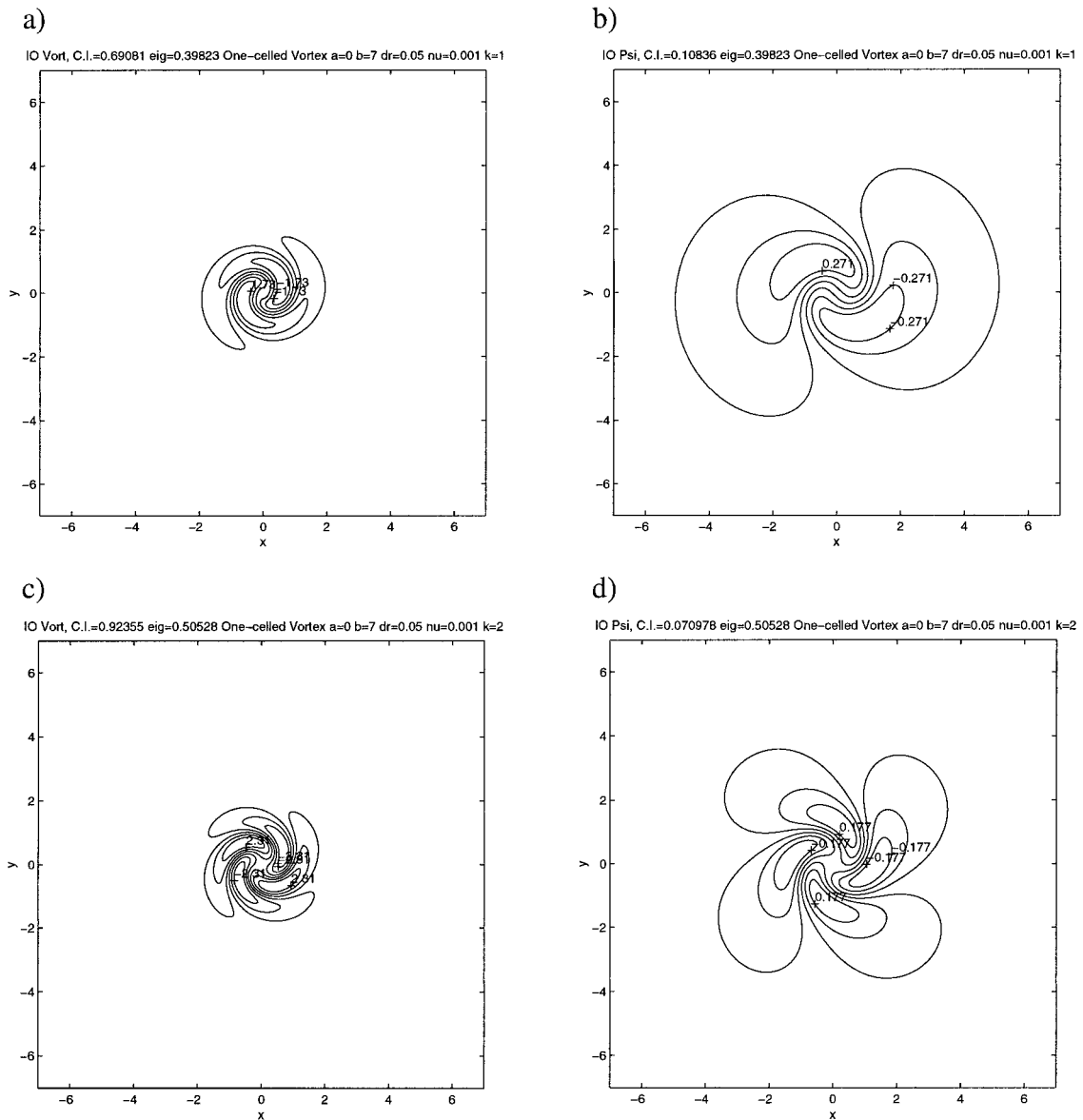


FIG. 8. The $k = 1$ and $k = 2$ IOs for the one-celled vortex: (a) $k = 1$ vorticity; (b) $k = 1$ streamfunction; (c) $k = 2$ vorticity; (d) $k = 2$ streamfunction. The contour intervals and energy growth rates (eigenvalues) are indicated at the top of each plot.

(1984); however, their analysis relied on a low-Reynolds number expansion, which clearly has limited application to atmospheric vortices or to our one-celled vortex with $Re_v = 1000$. Figure 3 shows the real part of the eigenvalue of the LDM for each azimuthal wavenumber from $k = 1$ to $k = 15$, for three cases: 1) with the radial inflow effects included, 2) with the stretching term [S in (4.3)] eliminated, and 3) with both the stretching and radial advection terms [S and $-UD_{up}$ in (4.3)] eliminated. We can see that for all three cases the one-celled vortex is asymptotically stable and the trend of the plot suggests that no unstable modes exist for any azimuthal wavenumber. The decay rate of these modes is clearly

linear with respect to azimuthal wavenumber, with the exception that the $k = 1$ decay rate appears exceptionally smaller than the trend of the other LDM decay rates would indicate. This decay rate linear in k indicates that it is the interaction with the shear of the swirling flow, rather than diffusion, that contributes most to the decline of the amplitudes of these modes.

Figure 3 also shows that the growth rates of the LDMs in all three cases are virtually identical for all $k > 1$. The reasons for this will be explained shortly. For $k = 1$, however, we have two additional observations: 1) removing the stretching term substantially decreases the growth rate of the LDM, and 2) removing completely

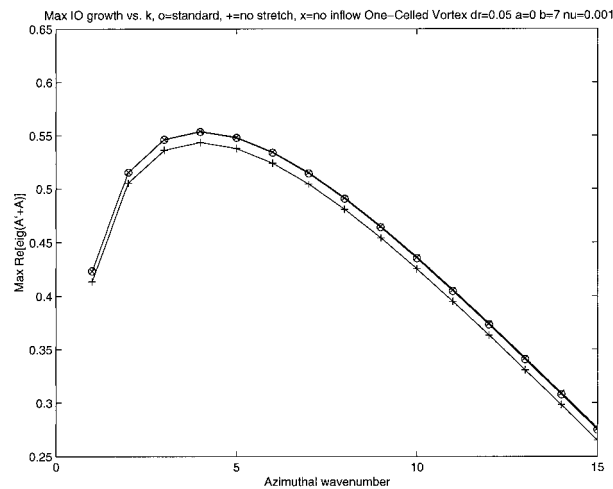


FIG. 9. The IO growth rates for $k = 1$ to $k = 15$ in the one-celled vortex: ○—standard case with inflow; +—with stretching term removed; ×—with stretching and advection removed.

the effects of radial inflow greatly increases the growth rate, from -2.5×10^{-3} to -2.65×10^{-6} (i.e., almost to neutrality).

The two vortex flows we have constructed have cylindrical deformation fields that have two distinct effects on the perturbation vorticities. First, the radial inflow advects perturbation vorticity into the vortex core (and outward from the axis in the two-celled vortex). Second, the associated deformation field can cause either vorticity amplification (through stretching) or vorticity decay (through compression). A comparison of the amplification rate due to vortex stretching with the actual growth rates suggests that the stretching/amplification associated with the radial inflow does play a role in the dynamics. In the case of the one-celled vortex, the maximum stretching rate of 0.005 (see Fig. 1c) is indeed comparable to the change that results when the stretching is eliminated from the dynamics.

Figure 4 shows vorticity and streamfunction contour plots of the LDM for the first two azimuthal wavenumbers (when the effects of radial inflow are included). These two modes are considerably different. For $k = 1$, the LDM is a dipole-like structure whose vorticity lies entirely inside the core of the vortex. For $k = 2$, the LDM lies at the outer edge of the domain and spirals inward in the same direction as the mean flow. In fact, the LDMs for all higher wavenumbers are higher-wavenumber replicas of the $k = 2$ LDM.

Why is the $k = 1$ LDM distinct from those of all higher wavenumbers? There are two reasons. First, $k = 1$ perturbations experience considerably less dissipation near $r = 0$ than higher wavenumber perturbations—this is due to the $-k^2/r^2$ term in the diffusive part of (4.3). Second, the perturbation velocities do not go to zero at $r = 0$, which is to say that only for $k = 1$ can there be perturbation flow across the $r = 0$ axis. In the case of the one-celled vortex, this allows the $k = 1$ LDM to

convert more mean-flow vorticity to perturbation vorticity, thereby helping to sustain itself. It is for these reasons that the decay rate of the $k = 1$ LDM is so small, especially when the radial inflow is neglected.¹ Because the higher wavenumber perturbations are therefore generally not well suited to persist in the core of the vortex, their LDMs lie instead as far away from the core as possible so that they are subjected to as little diffusion and deformation as possible. For this reason, the structures and locations of the LDMs for $k = 2$ and higher are entirely dependent on the location of the outer boundary of the domain. The fact that the LDMs for $k > 1$ lie near the outer boundary also explains why eliminating the effects of radial inflow has no noticeable effect on the growth rates—the stretching and advection are nearly zero in this region (see Fig. 1).

b. The stability of the two-celled vortex

We turn our analysis now to the two-celled vortex described in section 3c. Figure 5 shows the real parts of the eigenvalues of the LDMs for azimuthal wavenumber $k = 1$ through $k = 15$, where we have again also plotted the same results with stretching removed and with all radial inflow effects removed. For the case with inflow, there is a range of instability from $k = 3$ to $k = 10$. This is a “classic” result, which has been produced in many previous studies of the stability of rotating flows, particularly Staley and Gall (1979), Gall (1985), Steffens (1988), and Peng and Williams (1991). Our curve is slightly different from these earlier results due to the presence of diffusion, so that the stable modes are not neutral but rather have negative growth rates outside the unstable range.

It is interesting to note that removing the stretching term increases the growth rate for $k = 1$ and actually destabilizes the vortex for $k = 2$, yet substantially decreases the growth rates in the previously unstable range $3 \leq k \leq 10$. Removing both the stretching and the advection destabilizes the vortex for $k = 1$ and $k = 2$, but again decreases the growth rates for $3 \leq k \leq 10$. The growth rates for $k > 10$ are unaffected by radial inflow, and this is again due to the fact that the LDMs for these wavenumbers lie near the outer boundary where there is virtually no stretching or advection.

The vorticity and streamfunction fields for the most unstable (least damped) mode for the first azimuthal wavenumber with instability, $k = 3$, and the most un-

¹ Note added in proof: The LDM for $k = 1$ in the one-celled vortex is in fact a slightly modified version of the stationary solution for wavenumber one perturbations found by Michaelke and Timme (1967) for unbounded domains, which is a disturbance whose streamfunction is proportional to the mean flow velocity. Such a disturbance represents a linear displacement of the vortex center, and is sometimes called the “pseudo-mode” in the literature. The modification in our case is caused by the introduction of an outer boundary, which causes the mode to have a nonzero angular velocity.

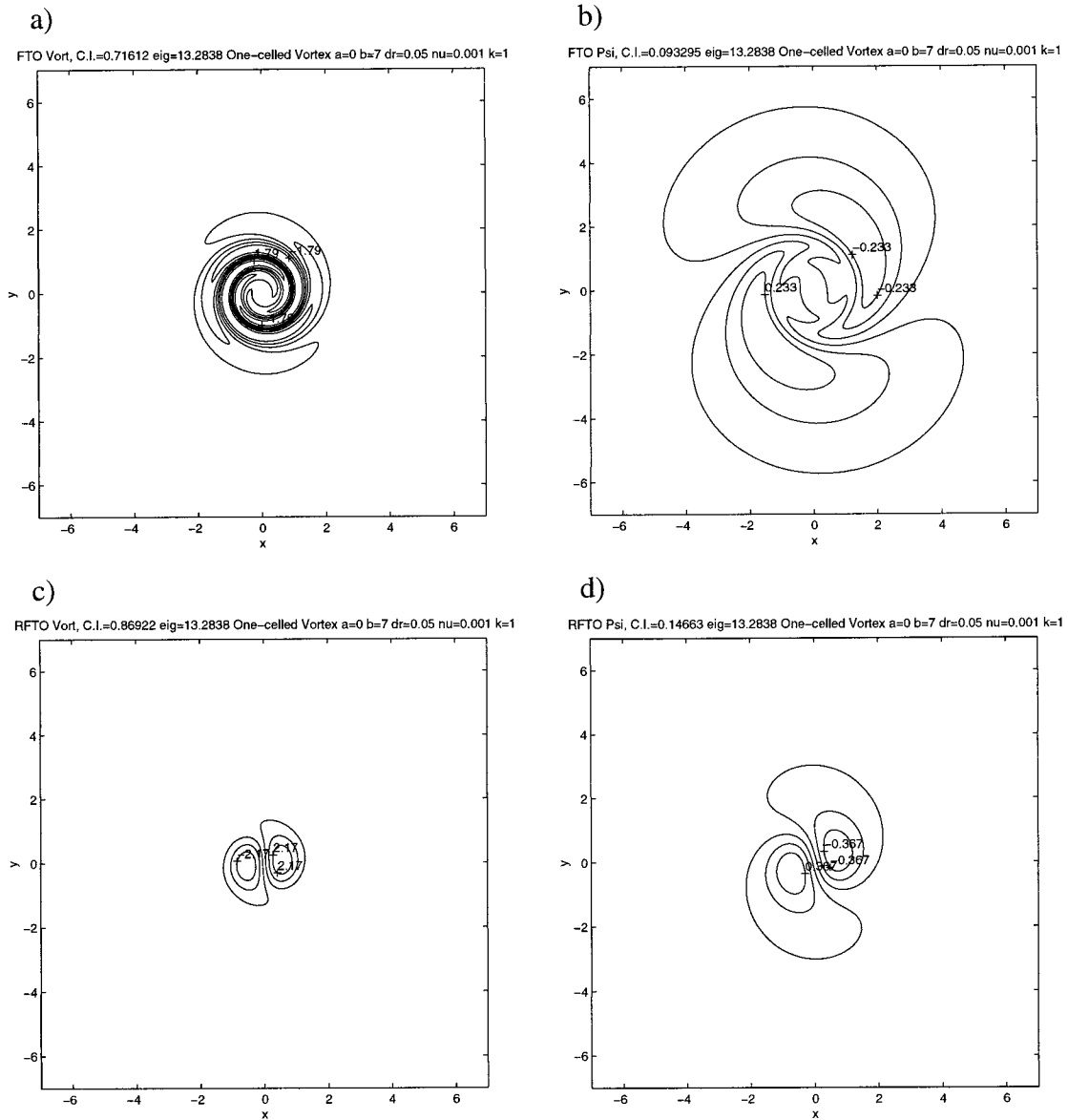


FIG. 10. Vorticity and streamfunction fields for the $k = 1$ FTO for $t = 8.98$, and its associated RFTO: (a) $k = 1$ FTO vorticity, (b) $k = 1$ FTO streamfunction, (c) $k = 1$ RFTO vorticity, (d) $k = 1$ RFTO streamfunction.

stable wavenumber, $k = 5$, are shown in Fig. 6. These modes are quite similar in structure, consisting of two concentric rings of ellipse-shaped vorticity perturbations, alternating in sign, located in the transition region between $r = 1$ and $r = 2$, with the two rings of perturbations shifted in phase from each other such that the inner rings lead the outer rings by almost exactly half a cycle. These modes operate with a mechanism that is the same as the two-dimensional modes identified in the earlier vortex stability studies noted above—see, in particular, Staley and Gall (1979), Gall (1983), and Flierl (1988). That is to say, they persist and/or grow through the familiar mechanism of converting mean flow vorticity to perturbation vorticity

via the $u_k(\partial Z/\partial r)$ term in (4.3). In Fig. 7, the modes show another common aspect of classical instabilities in that the angular velocity (phase speed) of the unstable modes is representative of the mean flow angular velocity in the transition zone, while the decaying modes have a much lower angular velocity: for $k = 1$ and $k = 2$, this is because the modes are retrograding against the mean flow, while for $k > 10$ it is because the modes lie near the outer boundary where Ω is small. The maximum angular velocity V/r in the two-celled vortex is $\Omega = 0.23$, while halfway through the transition region the angular velocity is $\Omega = 0.15$, which compares very favorably with the phase speeds of the unstable modes.

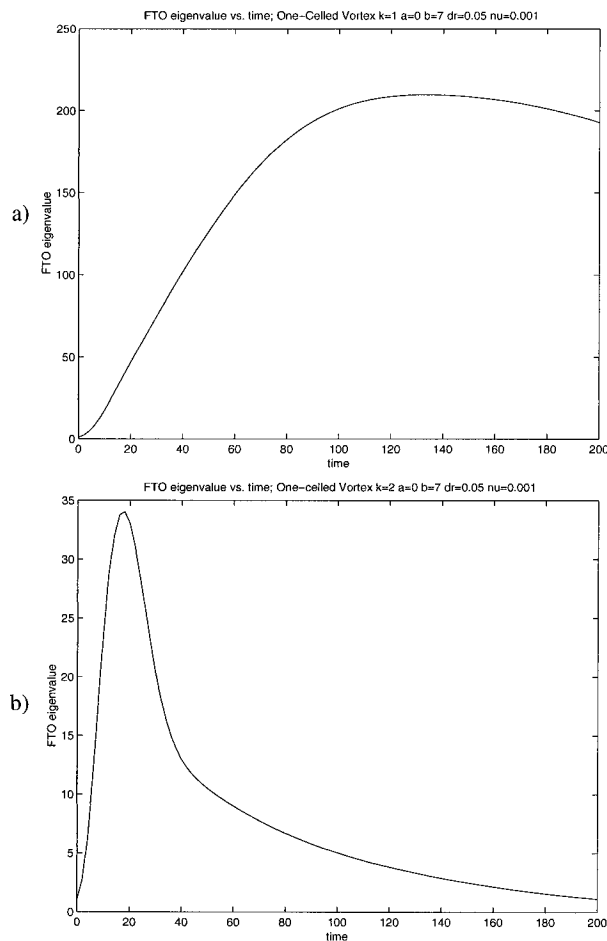


FIG. 11. FTO growth vs allowed growth time in the one-celled vortex for (a) azimuthal wavenumber $k = 1$; (b) $k = 2$.

6. Optimal growth perturbations

As Orr (1907) originally observed, the growth of a perturbation in linear, inviscid shear flow is determined solely by how far back against the shear the disturbance is originally tilted. A perturbation whose phase lines are tilted all the way back becoming nearly parallel with the flow could conceivably have unlimited growth. In more realistic flows this is prevented by diffusion. With this in mind, it is easy to imagine that the perturbation that would grow the most in an asymptotically stable inviscid vortex without radial inflow would be a vorticity perturbation that spirals back against the flow at an angle such that azimuthal advection would uncoil the vorticity of the perturbation, reducing its radial wavenumber until the vorticity contours were radially aligned at the moment of maximum perturbation amplitude. Viscosity would limit the possible maximum growth of such a perturbation: the tighter the spiral (in either direction) made by the perturbation, the faster viscosity would diffuse the vorticity.

The structures of IOs are usually quite different. The

IOs seek out the part of the flow that has the most shear or deformation, and arrange the vorticity there to create the fastest possible instantaneous growth in perturbation energy. This is usually a structure that locally tilts back against the shear of the flow at an angle of 45° , a geometry that maximizes the eddy fluxes $\overline{u'v'}$, and at the same time places the perturbation in the orientation leading to the maximum rate of decrease in wavenumber from advection by the local diffluent component of the shearing velocity field.

a. Instantaneous and finite-time optimals in the one-celled vortex

Figure 8 shows the vorticity and streamfunction fields for the $k = 1$ and $k = 2$ IOs on our one-celled vortex. We can see these perturbations have structures very much like those predicted above: the vorticity contours spiral back against the shear of the mean flow. The streamfunction contours show that the perturbation velocities flow back against the shear of the vortex at the expected angle of 45° , which maximizes the eddy fluxes, and the place where this occurs is in the vicinity of $r = 1$, where the maximum shear exists (note that in a vortex, the “shear” is not the rate of change of velocity $\partial V/\partial r$ but rather the rate of change of angular velocity $\partial\Omega/\partial r$). The $k = 2$ IO is essentially a higher-wavenumber replica of the $k = 1$ IO, and this was found to be true for all wavenumbers. The normalized IO growth rates for $k = 1$ through $k = 15$ are shown in Fig. 9, again for the three cases examined in our discussion of stability: with the radial inflow, without the stretching, and without the radial inflow. The growth rate (with inflow) increases from 0.42 at $k = 1$ to 0.55 at $k = 4$ and then quickly decreases. While such growth rates are known in inviscid flows to increase asymptotically with wavenumber toward a limit determined by the maximum deformation of the mean flow (Howard 1972), the decline after $k = 4$ in our vortex is caused by the increasing effects of viscosity on higher-wavenumber structures. Figure 9 also indicates that the stretching and advection terms make very little contribution to the transient growth process, which is due to the fact that the deformations of the mean radial and vertical velocities are two orders of magnitude smaller than the shear of the mean azimuthal velocities. The fact that the elimination of the advection terms seems to nearly cancel the effect of eliminating the stretching term is very likely due to the fact that by incompressibility (3.5) these terms must be equal in magnitude.

Figures 10a,b show the vorticity and streamfunction for the $k = 1$ FTO for a transient growth time of $t = 8.98$. This corresponds to the time it takes for the mean flow to travel one circuit around the vortex at $r = 1$. We again see the expected result that the perturbation spirals back against the mean flow, and it does so almost exactly once. We also note, however, that the vorticity of the FTO lies not in the immediate vicinity of $r = 1$ but rather

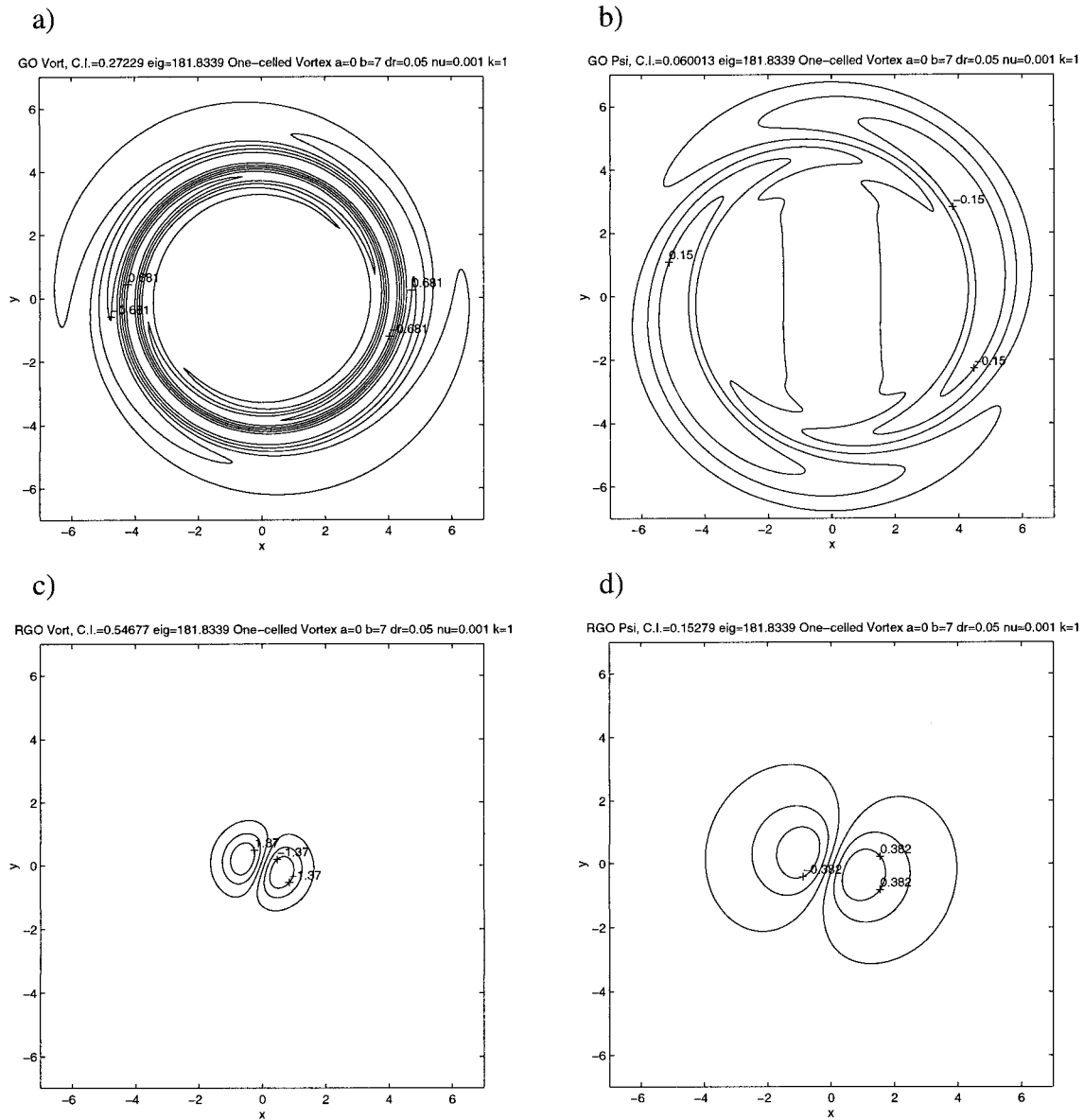


FIG. 12. Initial and fully realized states of the global optimal for $k = 1$ in the one-celled vortex: (a) GO vorticity, (b) GO streamfunction, (c) RGO vorticity, (d) RGO streamfunction.

at a small distance outside of $r = 1$. This displacement is indicative of the effect of radial inflow: as the vorticity is uncoiled, it is also carried inward toward $r = 1$. Figures 10c,d show the structure of this perturbation when it has reached its maximum energy at $t = 8.98$; we call this structure the *realized finite time optimal* (RFTO), and obtain it from the SVD of the propagator as outlined in section 2. This confirms the hypothesis that the perturbation reaches its maximum energy when the vorticity contours have been completely uncoiled, and it also shows that the radial inflow has carried the vorticity into the core of the vortex during this process.

Figure 11 shows the maximum transient growth in

energy as a function of time for $k = 1$ and $k = 2$ perturbations in the one-celled vortex. For $k = 1$, the maximum possible normalized energy growth is a factor of 181, which occurs at the time of $t = 131$; the perturbation that realizes this growth is called the *global optimal* (GO), and its maximal state will be called the *realized global optimal* (RGO). We see that the potential for transient growth of $k = 2$ perturbations is substantially less than that of $k = 1$ perturbations, with a maximum potential growth factor of only 33 occurring at $t = 17$. The GO for $k = 1$, and its realization, are shown in Fig. 12. The GO is a structure whose vorticity spirals far back against the mean flow, and it lies in the vicinity

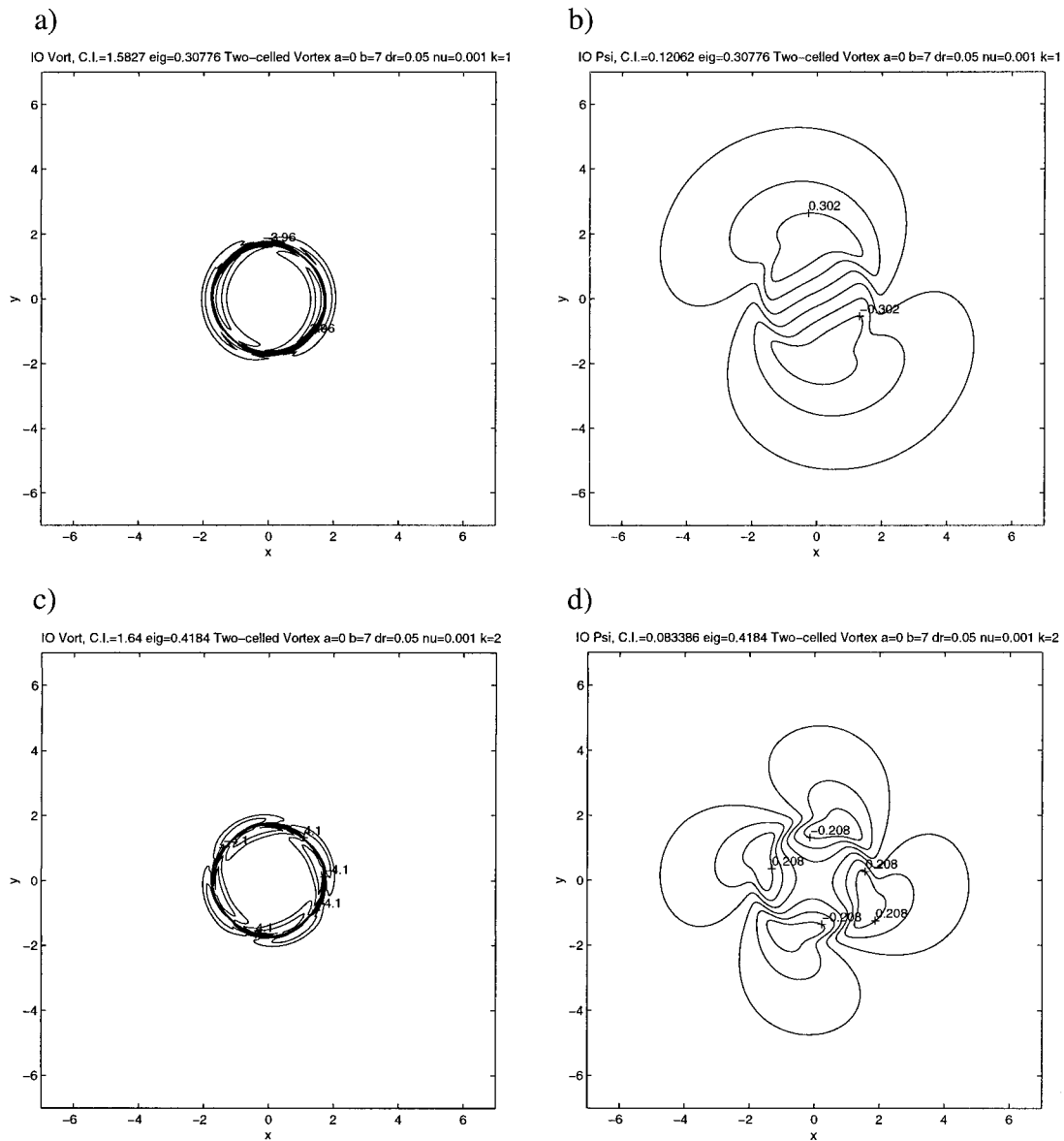


FIG. 13. Vorticity and streamfunction fields for the $k = 1$ and $k = 2$ IOs in the two-celled vortex: (a) $k = 1$ IO vorticity, (b) $k = 1$ IO streamfunction, (c) $k = 2$ IO vorticity, (d) $k = 2$ IO streamfunction.

of $r = 5$, which is the furthest extent of the field of substantial inflow velocities (see Fig. 1a), while the RGO shows again that this perturbation reaches its maximum energy when its vorticity has been advected into a dipolelike structure in the core of the vortex.

b. IOs and FTOs in the two-celled vortex: The stable regime

As we saw above, the two-celled vortex we have generated is stable for azimuthal wavenumbers $k = 1$, $k = 2$, and $k > 10$. Thus we can expect that wave-mean flow interactions at these stable wavenumbers will be

dominated by the optimal transients. Figure 13 shows the IOs for $k = 1$ and $k = 2$. The vorticities of these perturbations are again arranged to create downgradient eddy fluxes at the location of the maximum shear in the mean flow, which lies in the center of the transition zone between the exterior potential flow and the stagnant interior. Figure 14 shows the IO growth rates for azimuthal wavenumbers $k = 1$ through $k = 15$, including the cases with no stretching and with no radial inflow. Comparison with Fig. 5 indicates that the transient optimals can grow faster than their corresponding LDMs for all wavenumbers, even when unstable modes are present (note that the rate of energy increase is equal

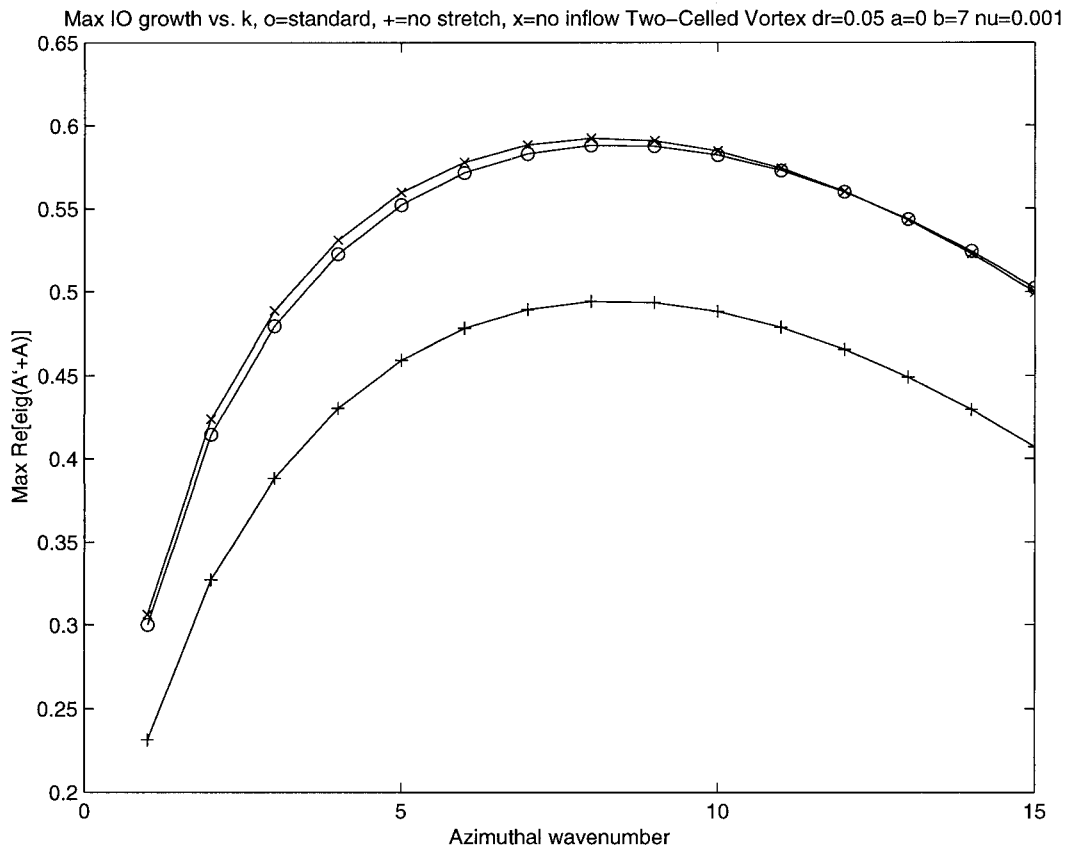


FIG. 14. Maximum instantaneous growth rates vs wavenumber for the first 15 azimuthal wavenumbers in the two-celled vortex: ○—standard case with inflow, +—with stretching term removed, ×—with stretching and advection removed.

to twice the modal growth rate). We also see that in the two-celled vortex, removal of the stretching term has a significant effect on the growth rate; this is due to the fact that the stretching term is only one order of magnitude (rather than two as before) less than the shear of the mean azimuthal velocities. We also see again that the elimination of advection nearly balances the elimination of stretching.

Figure 15 shows the maximum transient growth as a function of time for $k = 1$ and $k = 2$ in the two-celled vortex. While the growth in energy by a factor of 94 for $k = 1$ is substantial, the growth by a factor of 2886 for $k = 2$ is tremendous. The initial and maximal states of the $k = 2$ GO can be seen in Fig. 16 (these structures for $k = 1$ were similar). The initial state is the familiar reverse spiral, also displaced outward from the vortex core, like those we saw for the one-celled vortex. The maximal state, however, is considerably different than those we saw in the one-celled vortex. Rather than forming into a coherent quadrupole structure (which we might expect for the maximal state of a wavenumber two optimal), the GO evolves into a structure whose vorticity field is a lower-wavenumber version of the unstable modes (see Fig. 6). Why does this occur? As the GO

is deformed and advected into the vortex core, it interacts with the vorticity gradient of the mean flow. As it does so, it converts mean-flow vorticity into perturbation vorticity, thereby modifying the structure it would have if the only effect of the mean flow were deformation of the perturbation vorticity field. While *any* initial perturbation in *any* linearized system will indeed be dominated by the LDM in the limit as $t \rightarrow \infty$, the reason that we find such large transient growth for low wavenumbers in the two-celled vortex is that the energy acquired from the mean flow via the Orr mechanism accumulates in these very persistent LDMs, rather than being returned to the mean flow as the perturbation is sheared over. This result is very similar to what was found by Smith and Montgomery (1995) in their analysis of evolving disturbances in an unbounded Rankine vortex: as an initial disturbance is sheared over, much of its energy can be trapped in discrete modes and persist for long times.

c. Transient and long-term growth in the unstable regime

Are transient growth processes relevant in the unstable regime? Since the eigenvectors of \mathbf{T}_k (for each par-

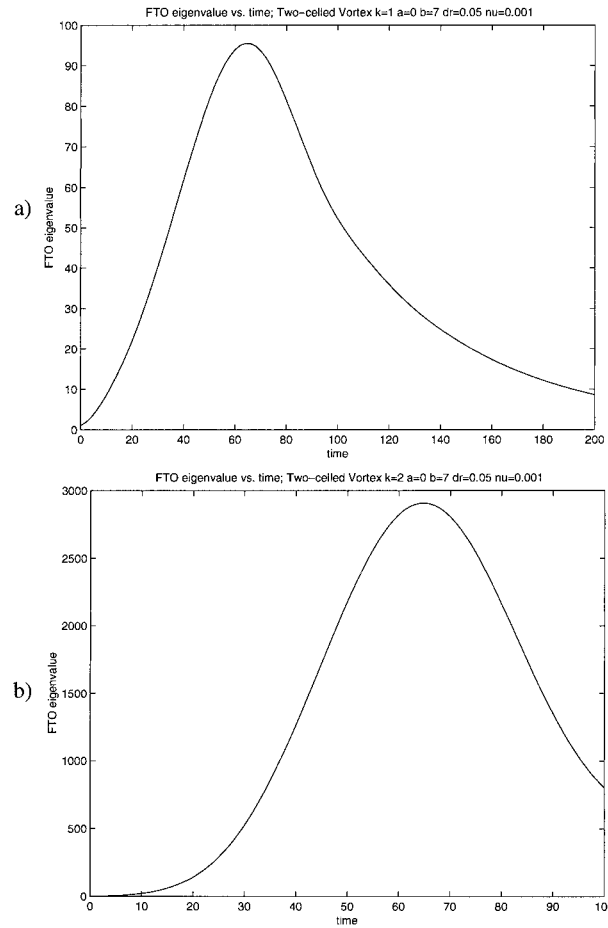


FIG. 15. FTO growth as a function of allowed growth time in the two-celled vortex: (a) azimuthal wavenumber $k = 1$, (b) $k = 2$.

ticular wavenumber k) are not orthogonal to each other, an arbitrary perturbation will almost surely project to some extent onto the most unstable mode, thereby exciting an exponentially growing perturbation. The total perturbation will then be asymptotically dominated by the unstable LDM. For linear systems with normal dynamical operators, the initial condition that achieves the greatest long-term growth would not surprisingly be the LDM itself. It is interesting to note, however, in non-normal systems such as these vortex/shear flows, the perturbation that excites the LDM the most for all times is not the LDM itself, but rather the LDM of the adjoint operator \mathbf{A}^\dagger (hereafter referred to as the LDMA). This was remarked by Farrell (1988) for neutral Rossby waves, but the argument is general and has been further discussed by Farrell and Ioannou (1996).

To see this mathematically, first recall that the solution in time to our linear dynamical system in generalized velocity coordinates (2.5) is

$$x(t) = e^{\mathbf{A}t}x(0). \quad (6.1)$$

Now consider the following standard diagonalization of the propagator matrix

$$e^{\mathbf{A}t} = \mathbf{E}e^{\mathbf{D}t}\mathbf{E}^{-1}, \quad (6.2)$$

where \mathbf{D} is a diagonal matrix with the eigenvalues of \mathbf{A} on its diagonal and \mathbf{E} is a matrix whose columns are the eigenvectors of \mathbf{A} . We may assume that the eigenvalues and eigenvectors are ordered such that the LDM lies in the first column of \mathbf{E} and its eigenvalue is the first element of \mathbf{D} . For large times the resultant propagator matrix is dominated by the contribution of the dominant eigenmode, the LDM. Therefore,

$$\lim_{t \rightarrow \infty} e^{\mathbf{A}t}_{kl} = \mathbf{E}_{k1}e^{\mathbf{D}_{11}t}\mathbf{E}_{1l}^{-1}. \quad (6.3)$$

The dominance of the LDM is indicated by the fact that it is the only one of the eigenvectors of \mathbf{A} that appears in this limit. What initial condition maximizes (in a normalized sense) the response of the LDM for large times? It is the one that maximizes its inner product with the rightmost term of (6.3). By Schwarz's inequality and our definition of the energy norm (2.6), this is the complex conjugate of the rightmost term, that is, $(\mathbf{E}_{1l}^{-1})^*$. Finally, since the diagonalization of the adjoint propagator is

$$e^{\mathbf{A}^\dagger t} = (\mathbf{E}^{-1})^\dagger e^{\mathbf{D}^\dagger t} \mathbf{E}^\dagger, \quad (6.4)$$

we observe that our desired initial condition is identical to the LDM of the adjoint of the dynamical operator \mathbf{A} .

Figure 17 shows the logarithm of the energy as a function of time for three $k = 3$ perturbations on the two-celled vortex: the LDM, the LDMA, and the FTO for $t = 5$. The LDM undergoes a steady exponential growth rate from $t = 0$ onward. The LDMA grows in energy even more rapidly than the LDM for a finite period of time, and then settles into the same exponential growth rate, but with 4.04 times as much energy at later times than the LDM. The FTO has an even faster initial growth rate, but after longer times has less energy than the LDMA. Examination of the LDMA and FTO vorticity and streamfunction fields, as shown in Fig. 18, is revealing. These structures are similar to the LDM in the vortex core, but outside of $r = 2$ they have the familiar reverse spiral. Thus we can see that their "extra" energy growth for short times comes from the transient growth associated with the uncoiling of the reverse spirals. We note that all the FTOs for growth times $t > 20$ (not shown) were identical to the LDMA. While for long times the structures that will dominate the perturbations for the unstable wavenumbers are indeed the unstable LDMs, the initial condition that leads the most rapid appearance of the LDM is in fact the LDMA.

7. Analysis

In this section we will examine two issues not directly addressed by the identification of the least damped

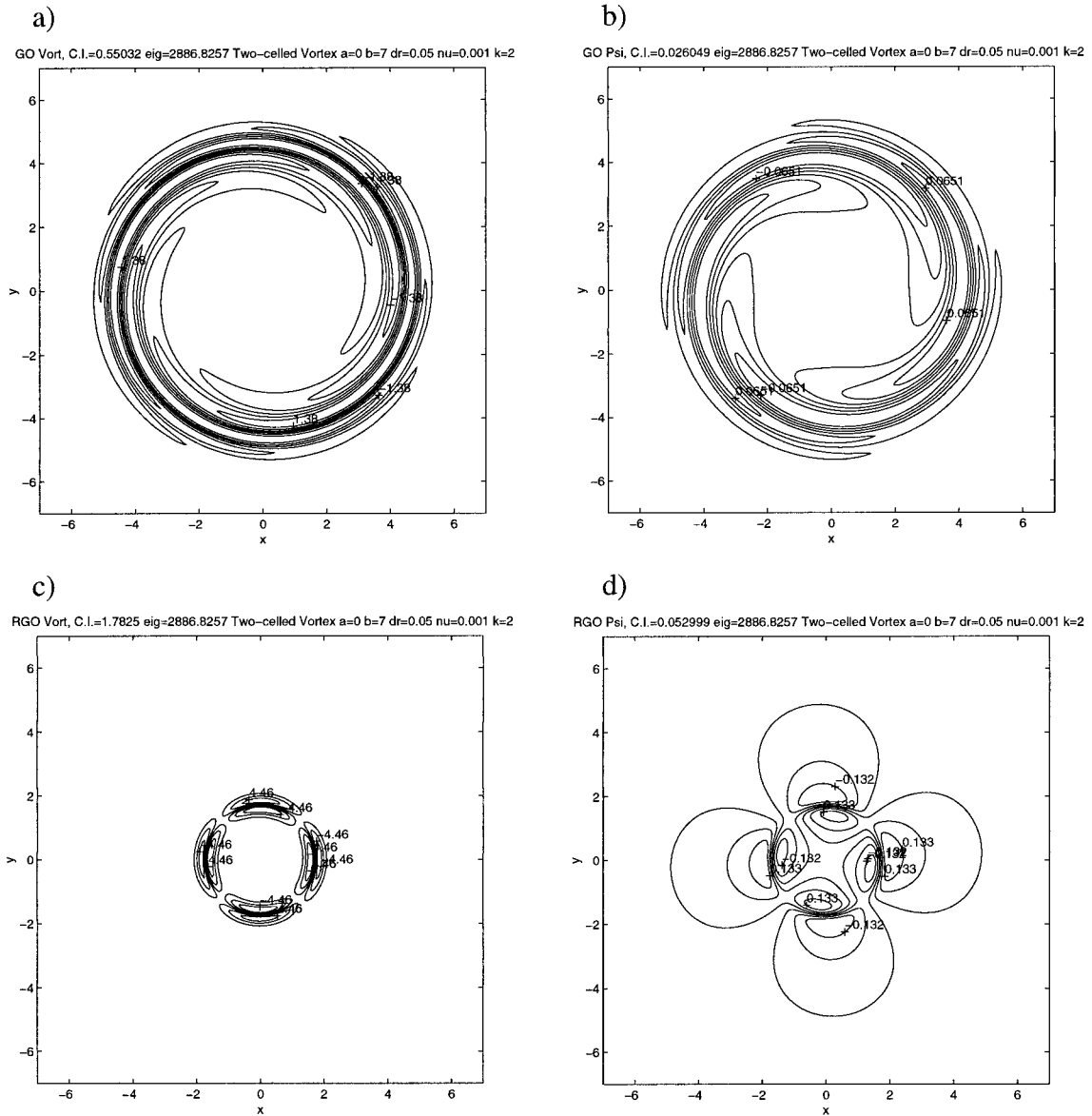


FIG. 16. Initial and maximal states of the GO for $k = 2$ on the two-celled vortex: (a) GO vorticity, (b) GO streamfunction, (c) RGO vorticity, (d) RGO streamfunction.

modes and/or the transiently growing optimals. The first issue will concern the exchange of energy between the perturbations and the mean flow, and the second issue will be the effect of radial inflow on transient growth processes.

a. Wave-mean flow interactions

Energy is exchanged between the mean flow and the perturbations via eddy fluxes. These eddy fluxes affect the mean flow through the divergence of the volume-averaged eddy flux terms (i.e., the Reynolds stresses) previously neglected in the mean flow equations such

as (3.6). The change to the mean azimuthal velocity caused by the perturbation eddy flux divergences is (Carr and Williams 1989; Montgomery and Kallenbach 1997)

$$\frac{\partial V}{\partial t} = -\frac{1}{r^2} \frac{\partial}{\partial r} \overline{(r^2 u' v')} = -\overline{u' \zeta'}, \quad (7.1)$$

where the overbars refer to azimuthal averages and the primes refer to the perturbation velocities and vorticities. These terms can be easily calculated to indicate—in the linear limit where we assume that the actual change of the mean flow is negligible—where the mean flow energy exchange is taking place and how the mean

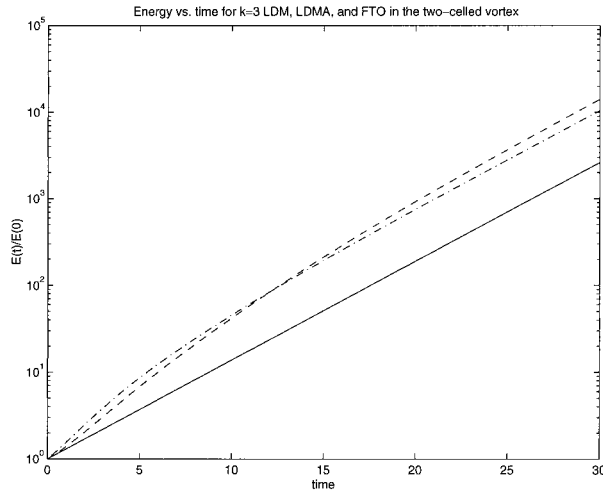


FIG. 17. Logarithms of the energies vs time of the LDM (solid), LDMA (dashed), and the $t = 5$ FTO (dash-dot) for azimuthal wave-number $k = 3$ in the two-celled vortex.

flow would indeed be changed if the perturbations were of substantial amplitude. The perturbations themselves, being asymmetric, have zero net momentum. They change the kinetic energy of the mean flow by rearranging its momentum via eddy momentum fluxes. Up-gradient (down-gradient) momentum fluxes cause an increase (decrease) in mean flow kinetic energy. This can be seen from examination of the equation for the rate of change of perturbation kinetic energy (for the case we are studying: strictly two-dimensional perturbations in cylindrically symmetric mean flows)

$$\frac{dE}{dt} = - \int_0^\infty \left[\overline{u^2} \frac{\partial U}{\partial r} + \frac{\overline{U}}{v^2} \frac{U}{r} + \overline{uv} \left(\frac{\partial V}{\partial r} - \frac{V}{r} \right) \right] 2\pi r dr, \quad (7.2)$$

where the overbars refer to the azimuthal averages. For convenience we have neglected the viscous damping terms. Another useful form of this equation can be found by integrating the first and third terms in the integrand of (7.2) by parts

$$\frac{dE}{dt} = \int_0^\infty \left[\left(\frac{\partial}{\partial r} \overline{u^2} + \frac{\overline{u^2}}{r} \right) U - \frac{\overline{U}}{v^2} \frac{U}{r} + \overline{u' \zeta'} V \right] 2\pi r dr, \quad (7.3)$$

where we have used (7.1) to simplify the third term in the integrand. This equation has a clear physical interpretation since the first and third terms now represent the products of the eddy flux divergences (which are accelerations) multiplied by the mean flow velocities, thereby indicating the interaction of the perturbations with the mean flow. The second term represents the work done by the mean flow against the centripetal forces associated with the perturbation azimuthal velocities. Note that it is always positive when U is negative. The

third term shows the direct interaction of the eddy flux divergence with the mean azimuthal flow. Since the rate of change of energy of the perturbations is equal and opposite to the rate of change of energy of the mean flow, this term clearly shows how up-gradient (down-gradient) momentum fluxes cause an increase (decrease) in the kinetic energy of the mean flow.

The eddy flux divergence of azimuthal momentum associated with the $k = 1$ IO in the one-celled vortex is shown in Fig. 19a. We can see that the immediate effect of the perturbation is to decelerate the mean flow inside r_{\max} and to accelerate the flow outside r_{\max} . The accumulated forcing of this perturbation over its lifetime can be found by simultaneously integrating the evolution of the perturbation (4.12) and the effect on the mean flow (7.1). We performed this integration from $t = 0$ to $t = 1000$, during which the energy of this perturbation decreased from $E = 1$ to $E = 0.005$. The accumulated forcing on the mean flow is shown in Fig. 19b, where we can see that the net effect of the wave-mean flow interaction for this perturbation over its lifetime is to decrease the azimuthal velocity in the vicinity of $r = 1$ and to increase it near $r = 0$ and near $r = 2$. [Note: this result should not be confused with the actual deviation of the mean flow velocities. The symmetric perturbations to the vortex flow caused by the eddy flux divergences will themselves evolve according to an advection-diffusion equation similar to (3.6). The behavior of these perturbations will be addressed in a future paper.]

The same calculation for the $k = 2$ IO in the one-celled vortex gives a different result. While we can see in Fig. 20a that the instantaneous effect of this perturbation at $t = 0$ is to decelerate the mean flow at $r = 1$, the long-term effect shown in Fig. 20b is to accelerate the flow near $r = 1$, such that the kinetic energy of the mean flow actually increases rather than decreases. Why is this result different? Shepherd (1985) and Farrell and Ioannou (1993a) have shown for inviscid linear shear flows that all perturbations, regardless of their initial configuration, are sheared over and give their energy to the mean flow via eddy fluxes. Equivalent results were found by Carr and Williams (1989) and Nolan (1996) for vortices with $1/r$ velocity profiles. Thus the net effect of any perturbation to these flows will ultimately be to increase the kinetic energy of the mean flow. However, if the mean flow has a background vorticity gradient, the transient perturbations may excite neutral or nearly neutral modes, such as the $k = 1$ LDM, which then serve as a trap for perturbation kinetic energy. In this case, the energy of transiently growing perturbations is never returned to the mean flow, but rather lost through dissipation of the perturbation instead. Our results here for the $k = 1$ and $k = 2$ IOs in the one-celled vortex are examples of each of these two possible outcomes.

In the two-celled vortex, the change in sign of the background vorticity gradient lends to the persistence or growth of coherent structures at all wavenumbers. Through investigation of many different initial condi-

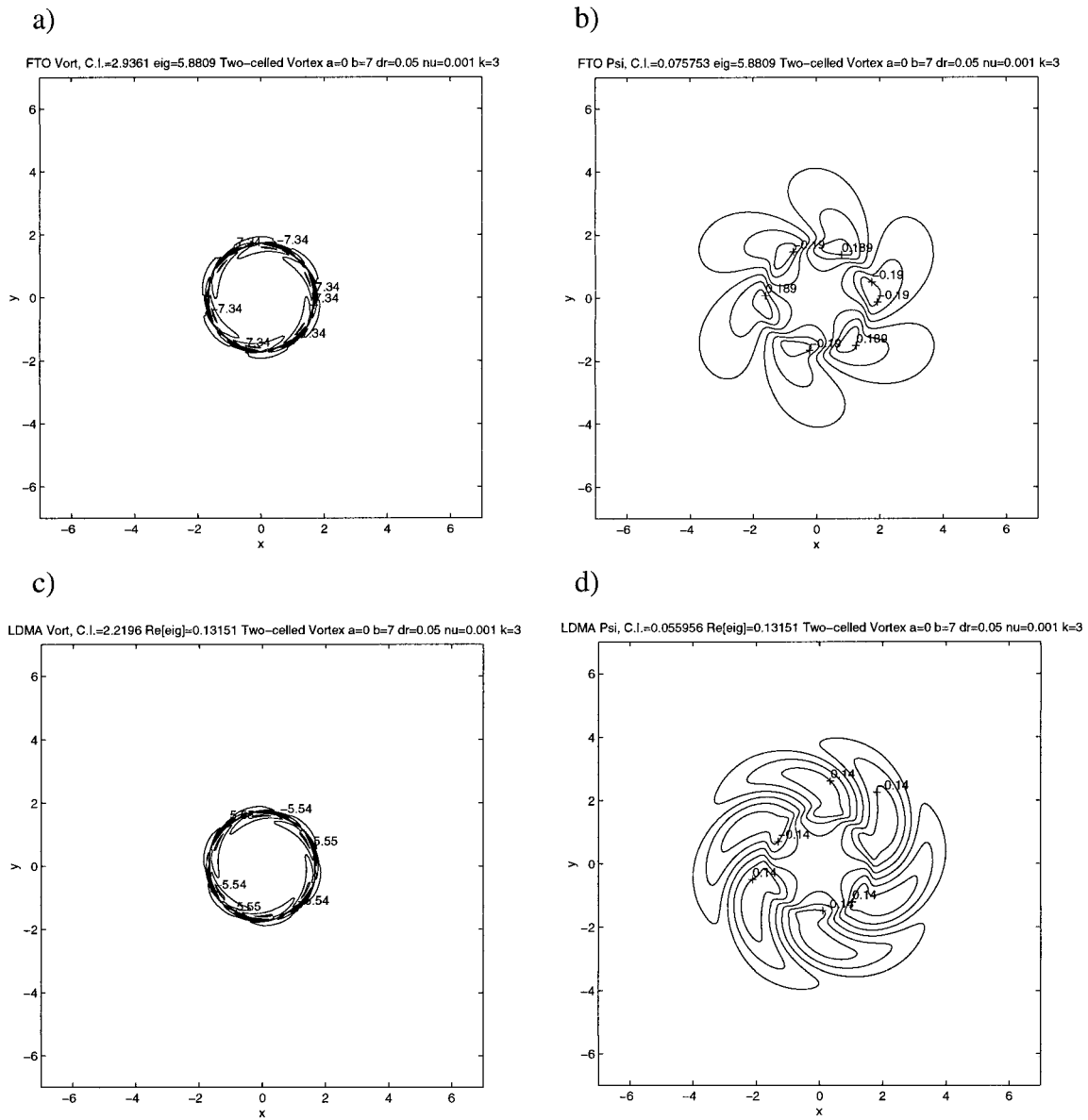


FIG. 18. Vorticity and streamfunction fields for the $t = 5$ FTO and the LDMA for $k = 3$ in the two-celled vortex: (a) FTO vorticity, (b) FTO streamfunction, (c) LDMA vorticity, (d) LDMA streamfunction.

tions, it appears that *any* perturbation initially configured to project favorably onto the LDM ultimately leads to a decrease in the kinetic energy of the mean flow. However, perturbations *can* be chosen that will ultimately lead to an increase in the kinetic energy in the mean flow. This is demonstrated in Fig. 21, where we have used as an initial condition the complex conjugate of the $k = 11$ IO in the two-celled vortex. Taking the complex conjugate results in a perturbation that spirals in the reverse direction, so that the initial eddy momentum flux is maximally upgradient rather than maximally downgradient. Since the $k = 11$ LDM is not as persistent as those at lower wavenumbers, the structure

is sheared over and the final result is a net upgradient flux of momentum and an increase in mean flow kinetic energy. For all lower wavenumbers with this special initial condition the opposite result was found.

b. The effects of radial inflow on transient growth

In previous sections we determined how accounting for the radial inflow changes the stability and optimal growth rates for perturbations in these vortices. However, it is perhaps more important to investigate how the stability of these vortices change as the strength of the deformation field changes. In the study of atmo-

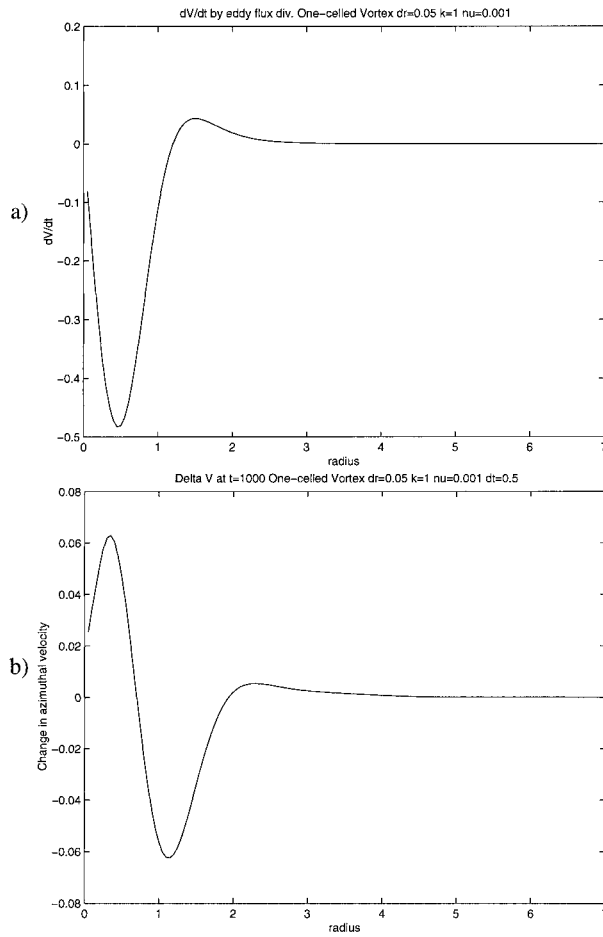


FIG. 19. (a) The instantaneous eddy momentum flux divergence of the $k = 1$ IO in the one-celled vortex. (b) The accumulated total momentum flux divergence from $t = 0$ to $t = 1000$ for the $k = 1$ IO.

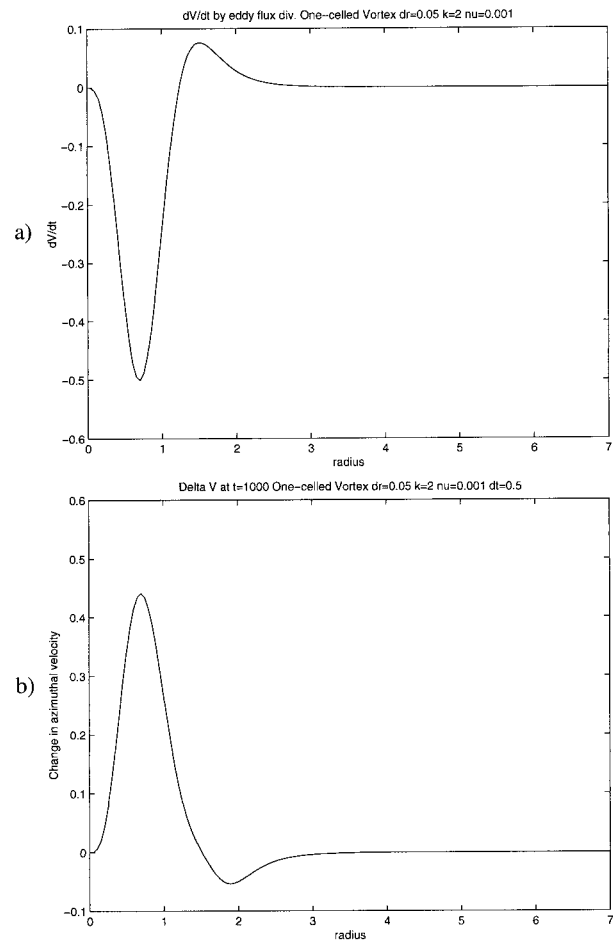


FIG. 20. (a) The instantaneous eddy momentum flux divergence of the $k = 2$ IO in the one-celled vortex. (b) The accumulated total momentum flux divergence from $t = 0$ to $t = 1000$ for the $k = 2$ IO.

spheric vortices it is practically assumed that a strong radial inflow will hold the vortex together, while a weaker inflow may allow the vortex to break apart. In our case we can examine how important the radial inflow is in stabilizing the vortex, as a function of the strength of the inflow itself. In the case of the one-celled vortex, a weaker radial inflow results in a broader, weaker vortex, that is, r_{\max} increases and v_{\max} decreases; a stronger radial inflow intensifies the vortex. In the case of the two-celled vortex, increasing the strength of the deformation field results in a sharper azimuthal velocity gradient in the transition zone from the potential flow to the stagnant core.

To determine the change in the potential for wave-mean flow interaction as the radial inflow varies, we have varied the strength of the radial inflow from half its original value to twice its original value, while recalculating the associated azimuthal velocity profile. For a radial inflow of half the original strength, we obtain an azimuthal velocity profile that is of the Burger's so-

lution type but with an increased $r_{\max} = 1.45$ and a decreased $v_{\max} = 0.5$; for twice the radial inflow we have $r_{\max} = 0.70$ and $v_{\max} = 1.01$. For each of these new vortex solutions we have recalculated both the maximum finite energy growth and this same growth when the radial inflow terms are neglected in the dynamics. The results of these calculations for $k = 1$ and $k = 2$ for the one-celled vortex are shown in Fig. 22. In both cases we see the following: first, neglecting the radial inflow terms results in a substantial overestimation of the maximum growth. Second, this overestimation increases as the strength of the radial inflow increases. Third, we find that for $k = 2$ and all higher azimuthal wavenumbers (not shown), the maximum growth (including the radial terms) begins to decrease when the radial inflow becomes strong enough.

Why does the presence of radial inflow velocity suppress transient growth? Indeed, this might seem paradoxical since increasing the radial inflow increases the maximum deformation rate of the mean flow. However,

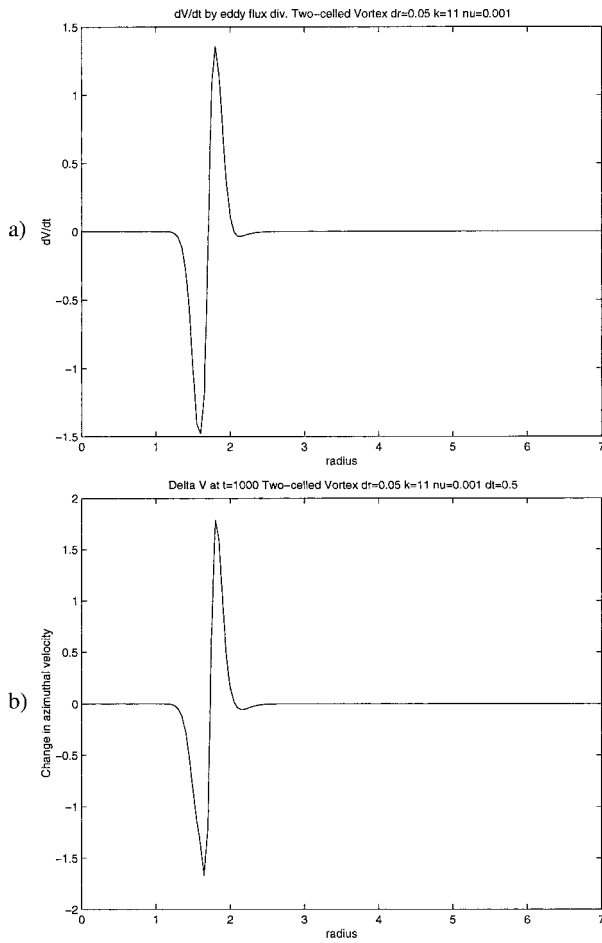


FIG. 21. (a) The instantaneous eddy momentum flux divergence of the complex conjugate of the $k = 11$ IO in the two-celled vortex. (b) The accumulated total momentum flux divergence from $t = 0$ to $t = 1000$.

the radial inflow also has the effect of advecting perturbation vorticity *through* the region of maximum shear, thereby limiting the extent of the wave–mean flow interaction.

Figure 23 shows similar calculations as above for $k = 1$ and $k = 2$ in the two-celled vortex. Since the two-celled vortex is unstable for these wavenumbers when radial inflow is neglected, we show the results only for the case with radial inflow. In this case we see again that the potential for transient growth begins to decline for larger relative intensities of the radial inflow. Similar calculations (not shown) for the high range of stable wavenumbers for the two-celled vortex, that is, $k > 10$, demonstrated that the maximum growth was underestimated by neglecting the radial inflow terms. This is because the mean vorticity to perturbation vorticity mechanism for growth is less effective for these higher wavenumbers and the radial deformation is a significant transient growth mechanism. However, the maximum growth for these wavenumbers is very small—on the

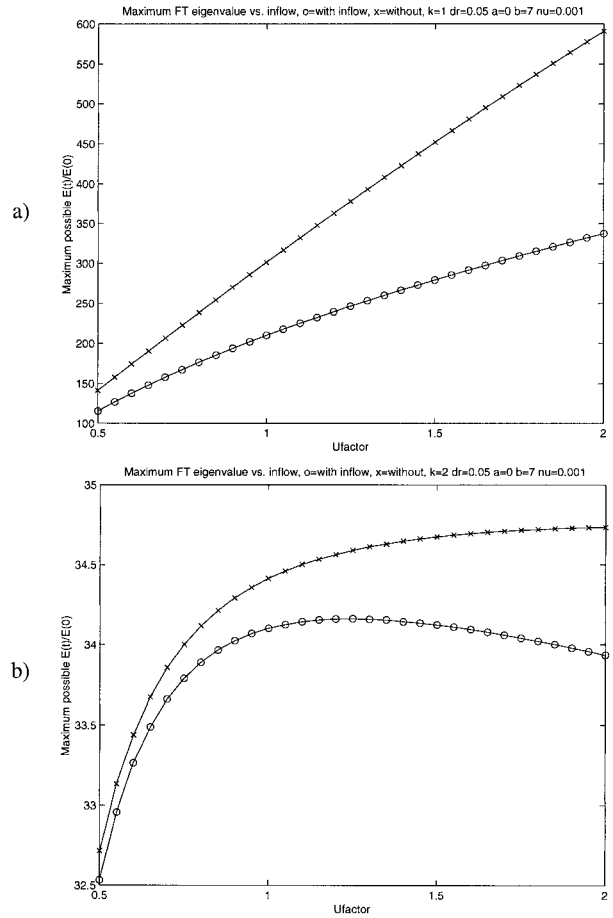


FIG. 22. Comparisons of the maximum transient growth in the one-celled vortex when the radial inflow terms are included (O's) or are not included (X's), as a function of the intensity of the radial inflow that maintains the swirling flow: (a) for azimuthal wavenumber $k = 1$; (b) for $k = 2$.

order of only a factor of 10 or less with increasing k , and the maximum growth calculated with the radial inflow terms was only 5%–10% more than without radial inflow.

8. Summary and conclusions

We have studied the dynamics of asymmetric perturbations in two-dimensional vortices that are maintained by radial inflow. The results we have found regarding stability are consistent with previous work on vortices of various velocity profiles: the one-celled vortex is stable for all azimuthal wavenumbers, while the two-celled vortex has a finite range of unstable wavenumbers due to the change in sign of the vorticity gradient of the mean flow. We also showed that the initial conditions that lead to the greatest perturbation energy for long times are not the most unstable modes but rather the most unstable modes of the adjoint operator.

For all wavenumbers in both vortices the fastest in-

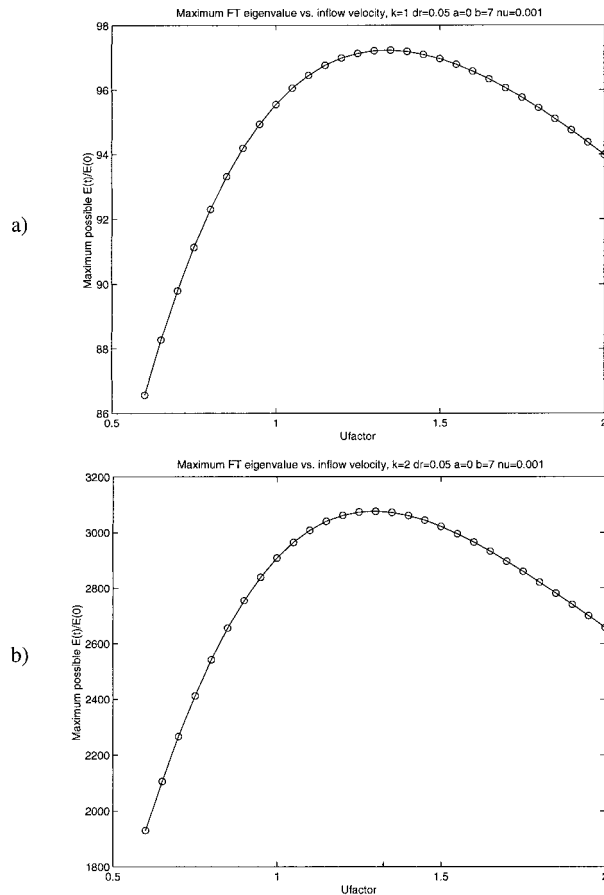


FIG. 23. The maximum transient growth in the two-celled vortex as a function of the intensity of the radial inflow that maintains the swirling flow: (a) for azimuthal wavenumber $k = 1$; (b) for $k = 2$.

stantaneous growth rates were shown to belong not to the LDMs but rather to the IOs. We also found that for stable wavenumbers substantial transient growth over finite times can occur for low-wavenumber perturbations in both the one-celled and two-celled vortex. The energy source for transiently growing perturbations is the exchange of energy with the mean flow via eddy momentum fluxes.

While the immediate effect of all growing perturbations is to decrease the kinetic energy of the mean flow, we found that the net effect of these perturbations on the mean flow over their lifetimes varies from case to case. While most initially growing perturbations result in a long-term decrease in the mean flow kinetic energy for all wavenumbers in the two-celled vortex, and for wavenumber $k = 1$ in the one-celled vortex, we found that most perturbations for $k > 1$ in the one-celled vortex ultimately increased the kinetic energy of the mean flow.

The effect of the radial inflow, generally neglected in previous stability analyses, was also investigated. The vortex stretching caused by the associated deformation field was found to stabilize wavenumber 2 perturbations

in the two-celled vortex despite the fact that the effect of the deformation field is to amplify perturbation vorticity. It was also found that the combination of both advection and deformation associated with the radial inflow was necessary to stabilize the two-celled vortex to wavenumber 1 perturbations. More relevant to the case of vortices being maintained by a radial inflow with intensity varying in time, we examined how the wave-mean flow dynamics changed as the azimuthal velocity field was adjusted to be in balance with changing radial inflow velocities. For all wavenumbers in the one-celled vortex, and for the low, stable wavenumbers in the two-celled vortex, we found that neglecting the radial inflow terms greatly overestimated the potential for transient growth or even destabilized the vortex completely. Furthermore, these measurable effects on asymmetric dynamics were found despite the fact that the maximum radial inflow velocities were at most only 10% of the maximum azimuthal velocities in the two-celled vortex and only 1% in the one-celled vortex.

There are two more important conclusions that can be drawn from our analyses. First, the potential for large transient growth of disturbances shows that a vortex need not be formally unstable before significant asymmetric structures, such as multiple vortices or polygonal eyewalls, can appear. Such disturbances may appear if, perhaps by chance, a disturbance is introduced into the vortex that projects favorably onto the optimal transients (i.e., it has an upshear tilt). Second, these favorably configured disturbances do not need to be introduced near the vortex core, but rather can be introduced in the near-vortex environment and still result in large wave-mean flow interaction (recall the global optimal shown in Figs. 12 and 16).

Throughout this investigation we have found that large transient growth in perturbation kinetic energy is limited to the lowest wavenumbers, in particular to only $k = 1$ for the one-celled vortex and both $k = 1$ and $k = 2$ for the two-celled vortex. Physically, $k = 1$ perturbations correspond to a linear displacement of some or all of the vorticity of the total flow. However, this translation is important since it corresponds to deviations in the path of the vortex, which has particularly important applications in the forecasting of hurricane tracks. It is also generally observed that tornadoes do not travel in straight lines (see, e.g., Fujita and Smith 1993) and even laboratory vortices (Wan and Chang 1972; Lund and Snow 1993) “wander” considerably, so it is possible that the transient growth and decay of wavenumber 1 perturbations is responsible for this phenomenon for both tornadoes and hurricanes. With this in mind we can see how generalized stability analysis could identify the characteristic features of disturbances that are most likely to cause significant changes in the path and intensity of tropical cyclones and tornadoes.

Acknowledgments. The authors would like to thank Prof. P. Ioannou, Prof. M. Montgomery, and Dr. T.

DelSole for many helpful discussions. We would also especially like to thank Dr. D. Adalsteinsson for helping us to make tremendous improvements in the production and appearance of our contour plots. Preliminary work for this report was prepared as part of the Ph.D. thesis of D. Nolan while he was a student at Harvard University, during which he was supported by NSF Grant ATM-9216813 and NSF Grant 9623539. Since November 1996 D. Nolan has been supported by the U.S. Department of Energy under Contract DE-AC03-76SF-00098. B. Farrell was supported by NSF Grants ATM-9216813 and 9623539.

REFERENCES

- Burgers, J. M., 1948: A mathematical model illustrating the theory of turbulence. *Adv. Appl. Mech.*, **1**, 197–199.
- Burggraf, O. R., K. Stewartson, and R. Belcher, 1971: Boundary layer induced by a potential vortex. *Phys. Fluids*, **14**, 1821–1833.
- Butler, K. M., and B. F. Farrell, 1992: Three dimensional optimal perturbations in viscous shear flows. *Phys. Fluids A*, **5**, 1390–1393.
- Carr, L. E., III, and R. T. Williams, 1989: Barotropic vortex stability to perturbations from axisymmetry. *J. Atmos. Sci.*, **46**, 3177–3191.
- Farrell, B. F., 1982: The initial growth of disturbances in a baroclinic flow. *J. Atmos. Sci.*, **39**, 1663–1686.
- , 1988: Optimal excitation of neutral Rossby waves. *J. Atmos. Sci.*, **45**, 163–172.
- , 1989: Transient development in confluent and diffluent flow. *J. Atmos. Sci.*, **46**, 3279–3288.
- , and P. J. Ioannou, 1993a: Stochastic forcing of perturbation variance in unbounded shear and deformation flows. *J. Atmos. Sci.*, **50**, 200–211.
- , and —, 1993b: Optimal excitation of three-dimensional perturbations in viscous constant shear flow. *Phys. Fluids A*, **5**, 1390–1400.
- , and —, 1996: Generalized stability theory. Part I: Autonomous operators. *J. Atmos. Sci.*, **53**, 2025–2040.
- Fiedler, B. H., 1994: The thermodynamic speed limit and its violation in axisymmetric numerical simulations of tornado-like vortices. *Atmos.–Ocean*, **32**, 335–359.
- , and R. Rotunno, 1986: A theory for the maximum wind-speeds in tornado-like vortices. *J. Atmos. Sci.*, **43**, 2328–2340.
- Flierl, G. R., 1988: On the instability of geostrophic vortices. *J. Fluid Mech.*, **197**, 349–388.
- Franklin, J. L., J. S. Lord, S. E. Feuer, and F. D. Marks Jr., 1993: The kinematic structure of Hurricane Gloria (1985) determined from nested analyses of dropwindsonde and Doppler radar data. *Mon. Wea. Rev.*, **121**, 2433–2451.
- Fujita, T. T., and B. E. Smith, 1993: Aerial survey and photography of tornado and microburst damage. *The Tornado: Its Structure, Dynamics, Prediction, and Hazards*, C. Church et al., Eds., American Geophysical Union, 1–17.
- Gall, R. L., 1983: A linear analysis of the multiple vortex phenomenon in simulated tornadoes. *J. Atmos. Sci.*, **40**, 2010–2024.
- , 1985: Linear dynamics of the multiple-vortex phenomenon in tornadoes. *J. Atmos. Sci.*, **42**, 761–772.
- Guinn, T. A., and W. H. Schubert, 1993: Hurricane spiral bands. *J. Atmos. Sci.*, **50**, 3380–3403.
- Howard, L. N., 1972: Bounds on flow quantities. *Annu. Rev. Fluid Mech.*, **4**, 473–493.
- Howells, P. A. C., R. Rotunno, and R. K. Smith, 1988: A comparative study of atmosphere and laboratory-analogue numerical tornado-vortex models. *Quart. J. Roy. Meteor. Soc.*, **114**, 801–822.
- Kallenbach, R. J., and M. T. Montgomery, 1995: Symmetrization and hurricane motion in an asymmetric balance model. Preprints, *21st Conf. on Hurricanes and Tropical Meteorology*, Miami, FL, Amer. Meteor. Soc., 103–105.
- Leibovich, S., and K. Stewartson, 1983: A sufficient condition for the instability of columnar vortices. *J. Fluid Mech.*, **126**, 335–356.
- Lewellen, W. S., and D. C. Lewellen, 1997: Large-eddy simulation of a tornado's interaction with the surface. *J. Atmos. Sci.*, **54**, 581–605.
- Liu, Y., D.-L. Zhang, and M. K. Yau, 1997: A multiscale numerical study of Hurricane Andrew (1992). Part I: Explicit simulation and verification. *Mon. Wea. Rev.*, **125**, 3073–3093.
- Lund, D. E., and J. T. Snow, 1993: Laser doppler velocimeter measurements in tornadolike vortices. *The Tornado: Its Structure, Dynamics, Prediction, and Hazards*, C. Church, D. Burgess, C. Doswell, and R. Davies-Jones, Eds., Amer. Geophys. Union, 297–306.
- Molinari, J., 1992: Environmental controls on eye wall cycles and intensity change in Hurricane Allen (1980). *Proc. ICSU/WMO Int. Symp. on Tropical Cyclone Disasters*, Beijing, China, World Meteorological Organization, 328–337.
- Montgomery, M. T., and R. J. Kallenbach, 1997: A theory for vortex Rossby waves and its application to spiral bands and intensity changes in hurricanes. *Quart. J. Roy. Meteor. Soc.*, **123**, 435–465.
- Nolan, D. S., 1996: Axisymmetric and asymmetric vortex dynamics in convergent flows. Ph.D. thesis, Harvard University, 279 pp. [Available from University Microfilm, 305 N. Zeeb Rd., Ann Arbor, MI 48106.]
- Orr, W. M., 1907: Stability or instability of the steady motions of a perfect liquid. *Proc. Roy. Irish Acad.*, **27**, 9–69.
- Peng, M. S., and R. T. Williams, 1991: Stability analysis of barotropic vortices. *Geophys. Astrophys. Fluid Dyn.*, **58**, 263–283.
- Rayleigh, Lord, 1880: On the stability and instability of certain fluid motions. *Proc. London Math. Soc.*, **11**, 57–70.
- Robinson, A. C., and P. G. Saffman, 1984: Stability and structure of stretched vortices. *Stud. Appl. Math.*, **70**, 163–180.
- Rott, N., 1958: On the viscous core of a line vortex. *Z. Angew. Math. Mech.*, **9**, 543–553.
- Rotunno, R., 1978: A note on the stability of a cylindrical vortex sheet. *J. Fluid Mech.*, **87**, 761–771.
- Schubert, W. H., M. T. Montgomery, R. K. Taft, T. A. Guinn, S. R. Fulton, J. P. Kossin, and J. P. Edwards, 1999: Polygonal eyewalls, asymmetric eye contraction, and potential vorticity mixing in hurricanes. *J. Atmos. Sci.*, **56**, 1197–1223.
- Shapiro, L. J., 1992: Hurricane vortex motion in a three-layer model. *J. Atmos. Sci.*, **49**, 401–421.
- Shepherd, T. G., 1985: Time development of small disturbances to plane Couette flow. *J. Atmos. Sci.*, **42**, 1868–1871.
- Smith, G. B., II, and M. T. Montgomery, 1995: Vortex axisymmetrization: Dependence on azimuthal wavenumber or asymmetric radial structure changes. *Quart. J. Roy. Meteor. Soc.*, **121**, 1615–1650.
- Smith, R. K., and H. C. Weber, 1993: An extended analytic theory of tropical-cyclone motion in a barotropic shear flow. *Quart. J. Roy. Meteor. Soc.*, **119**, 1149–1166.
- Staley, D. O., 1985: Effect of viscosity on inertial instability in a tornado vortex. *J. Atmos. Sci.*, **42**, 293–297.
- , and R. L. Gall, 1979: Barotropic instability in a tornado vortex. *J. Atmos. Sci.*, **36**, 973–981.
- , and —, 1984: Hydrodynamic instability of small eddies in a tornado vortex. *J. Atmos. Sci.*, **41**, 422–429.
- Steffens, J. L., 1988: The effect of vorticity-profile shape on the instability of a two-dimensional vortex. *J. Atmos. Sci.*, **45**, 254–259.

- Sullivan, R. D., 1959: A two-cell vortex solution of the Navier–Stokes equations. *J. Aerosp. Sci.*, **26**, 767–768.
- Thompson, W., 1887: Stability of fluid motion: Rectilinear motion of viscous fluid between two parallel planes. *Philos. Mag.*, **24**, 188–196.
- Wan, C. C., and C. C. Chang, 1972: Measurement of the velocity field in a simulated tornado-like vortex using a three-dimensional velocity probe. *J. Atmos. Sci.*, **29**, 116–127.
- Willoughby, H. E., 1992: Linear motion of a shallow-water barotropic vortex as an initial-value problem. *J. Atmos. Sci.*, **49**, 2015–2031.
- , 1995: Normal-mode initialization of barotropic vortex motion models. *J. Atmos. Sci.*, **52**, 4501–4514.